[redacted]CONFIDENTIAL

194
Copy
RM L55C22

NACA RM L55C22

7610

USAF TECHNICAL LIBRARY
HOLLOMAN AIR FORCE BASE
ALAMOGORDO, NEW MEXICO
28 SEP 1955

TECH LIBRARY KAFB, NM
0143574

NACA

RESEARCH MEMORANDUM

AN EVALUATION OF A ROLLERON-ROLL-RATE STABILIZATION SYSTEM FOR A CANARD MISSILE CONFIGURATION AT MACH NUMBERS FROM 0.9 TO 2.3

By Martin L. Nason, Clarence A. Brown, Jr.,
and Rupert S. Rock

Langley Aeronautical Laboratory
Langley Field, Va.

[redacted]

NATIONAL ADVISORY COMMITTEE
FOR AERONAUTICS

WASHINGTON

September 15, 1955

[redacted]CONFIDENTIAL

TECH LIBRARY KAFB, NM
0143574

NATIONAL ADVISORY COMMITTEE FOR AERONAUTICS

RESEARCH MEMORANDUM

AN EVALUATION OF A ROLLERON-ROLL-RATE STABILIZATION SYSTEM FOR A CANARD MISSILE CONFIGURATION AT MACH NUMBERS FROM 0.9 TO 2.3

By Martin L. Nason, Clarence A. Brown, Jr., and Rupert S. Rock

SUMMARY

A linear stability analysis and a flight-test investigation have been performed on a rolleron-roll-rate stabilization system for a canard missile configuration through a Mach number range from 0.9 to 2.3. This type of damper provides roll damping by the action of gyro-actuated uncoupled wing-tip ailerons. A dynamic roll instability predicted by the analysis was confirmed by flight testing and was subsequently eliminated by the introduction of control-surface damping about the rolleron hinge line. The control-surface damping was provided by an orifice-type damper contained within the control surface. Steady-state rolling velocities were at all times less than 1 radian per second between Mach numbers of 0.9 to 2.3 on the configurations tested. After the introduction of control-surface damping, no adverse longitudinal effects were experienced in flight because of the tendency of the free-floating rollerons to couple into the pitching motion at the low angles of attack and disturbance levels investigated herein.

INTRODUCTION

One of the problems frequently encountered in missile design is that of providing adequate roll damping. This problem is primarily a consequence of the predominance of low-aspect-ratio surfaces on missile configurations. Very often this problem is solved by a servomechanism which senses roll rate and actuates a control surface to give the necessary damping. Unfortunately, however, these servomechanisms require missile space and their inherent complexity tends to decrease the overall reliability of the missile. Recently, a unique, simple, and purely mechanical roll damper which requires no internal components was designed for missile applications. (See ref. 1.) Roll damping is achieved in this system by

independently acting wing-tip ailerons with enclosed airstream-impelled roll-rate-sensitive gyro wheels. The spin axis of the gyro wheel is perpendicular to the plane of the wing when the aileron is in the undeflected position. This type of roll damper is referred to as a rolleron. A stability analysis has been performed on a canard missile configuration on which this type of roll damper was installed. In order to determine the validity of the analytical approach adopted, a flight investigation was initiated and two research models were subsequently flown. Data obtained from these rocket-model tests confirmed the analysis and thus provided a reliable design approach for rolleron-type dampers on missile configurations.

SYMBOLS

L rolling moment, ft-lb

H rolleron hinge moment, ft-lb

φ missile roll angle, deg

δ rolleron angular deflection, radians

$\dot{\varphi}_m$ mean value of missile roll velocity, deg/sec

$L_{\dot{\varphi}}$ missile roll damping, $\frac{\partial L}{\partial \dot{\varphi}}$, ft-lb/radian/sec

L_δ rolleron control effectiveness parameter, $\frac{\partial L}{\partial \delta}$, ft-lb/radian

H_δ rolleron hinge-moment parameter, $\frac{\partial H}{\partial \delta}$, ft-lb/radian

$H_{\dot{\delta}}$ rolleron control-surface damping, $\frac{\partial H}{\partial \dot{\delta}}$, ft-lb/radian/sec

L_D load disturbance in roll, ft-lb

$C_{h_\delta} = \frac{H_\delta}{qSc}$

$C_{l_\delta} = \frac{L_\delta}{qSb}$

$$C_{l_p} = \frac{L_{\dot{\phi}}}{qS\left(\frac{b^2}{2V}\right)}$$

m	mass of rolleron, slugs
l	distance from missile longitudinal axis to arbitrary mass point in rolleron
d	distance from rolleron hinge line to arbitrary mass point in rolleron
$\bar{l}$	distance from missile longitudinal axis to rolleron center of gravity, ft
$\bar{d}$	distance from rolleron hinge line to rolleron center of gravity, ft
H_R	mass unbalance parameter, $\int_R l d\, dm = m\bar{l}\,\bar{d}$, slug-ft^2
I_X	moment of inertia of missile about longitudinal axis, slug-ft^2
I_R	moment of inertia of rolleron about hinge line, slug-ft^2
I_G	moment of inertia of rolleron gyro wheel about spin axis, slug-ft^2
ω_G	gyro-wheel angular velocity, radian/sec
H_G	angular momentum of gyro wheel, $I_G\omega_G$, slug-ft^2—radian/sec
$A_{\dot{\phi}}$	half amplitude of self-sustained roll-velocity oscillation, deg/sec
$\omega_{\dot{\phi}}$	frequency of self-sustained roll oscillation, cps
R	Reynolds number based on missile length
M	Mach number
V	missile velocity, ft/sec
q	dynamic pressure, lb/sq ft

ζ damping ratio of quadratic factor

S body cross-sectional area, 0.136 ft^2

c body diameter, 0.416 ft

b wing span, 1.75 ft

$D = \frac{d}{dt}$

A dot over a symbol denotes a derivative with respect to time.

ROLLERON OPERATION AND MISSILE ROLL SPECIFICATION

Operating Principle

A diagrammatic sketch of the roll-control system is shown in figure 1. The system consists of an aileron hinged near the leading edge. Enclosed in the aileron is a gyro wheel with the spin axis perpendicular to the plane of the wing in the undeflected aileron position. If the missile is undergoing a rolling velocity $\dot{\phi}$ indicated by the arrow, the aileron will be subjected to a gyroscopic hinge moment H. The gyroscopic hinge moment causes an aileron deflection which in turn creates a rolling moment L in a direction opposite to the initially assumed rolling velocity $\dot{\phi}$. As a result, resistance to rolling is produced and the roll damping of the missile is greater than the inherent aerodynamic roll damping by an amount determined by the roll effectiveness of the aileron. Obviously, the utility of this damper is determined by the amount of damping contributed to the missile without simultaneously introducing undesirable effects on the longitudinal motion and roll stability.

Roll-Performance Specifications

The assumed roll-performance specifications of the missile configuration tested herein which will serve as a criterion in evaluating the flight-test data, are:

(1) Flight condition: It is required that the missile fly at altitudes from sea level to 40,000 feet and at Mach numbers from 1.2 to 2.5.

(2) Static characteristics: The steady-state damped roll rate must be less than 1 radian per second.

(3) Dynamic characteristics: The rolleron system must be dynamically stable in the sense that any oscillatory modes present possess positive damping.

MODELS

Detailed sketches of the two test vehicles employed in this investigation are illustrated in figure 2 and photographs of the models are presented in figure 3. Model A (fig. 2(a)) differs from model B (fig. 2(b)) in that a control-surface damper about the aileron hinge line has been added to model B. A detailed discussion of the damper development and construction is included in a later section. Missile lifting and control surfaces are shown in figure 4. The canard surfaces had 66° 37' delta-wing plan forms with a modified single-wedge airfoil section of constant thickness. Wings were of trapezoidal plan form with the leading edge swept back 45°.

The experimentally measured mass, inertia, and damping characteristics of each model are given in table I. Slight changes in the parameters I_R, m, and $\bar{d}$ from model A to B were due essentially to the rolleron structural modifications necessary to increase the control-surface damping.

ROLLERON-SYSTEM STABILITY ANALYSIS

Equations of Motion

For analysis purposes it is assumed that the rolling motion is restricted to two degrees of freedom: (1) missile rotation about the longitudinal axis ϕ and (2) control-surface rotation about the hinge line δ. If it is further assumed that the aerodynamic forces and moments depend linearly on their respective variables and that the angular momentum vector of the gyro wheel is essentially perpendicular to the plane of the wing, the equations of motion may be expressed as follows:

Rolling moment:

$$L_D + L_{\dot{\phi}} \frac{\dot{\phi}}{57.3} + 4L_{\delta}\delta + 4H_R\ddot{\delta} + 4H_G\dot{\delta} = I_X \frac{\ddot{\phi}}{57.3} \tag{1}$$

Hinge moment:

$$H_\delta \delta + H_{\dot{\delta}} \dot{\delta} + H_R \frac{\ddot{\phi}}{57.3} - H_G \frac{\dot{\phi}}{57.3} = I_R \ddot{\delta} \tag{2}$$

The sign convention defining positive directions of moments and angles is shown in figure 5. Equation (2) applies to any one of the four ailerons, since each is undergoing a similar motion.

Static Relationships

Solving equations (1) and (2) for the ratio of applied rolling moment L_D to the steady-state rolling velocity $\dot{\phi}_{ss}$ and control-surface deflection δ_{ss}, respectively, results in the following equations:

$$\frac{-L_D}{\dot{\phi}_{ss}/57.3} = L_{\dot{\phi}} + \frac{4L_\delta}{H_\delta} H_G \tag{3}$$

$$\frac{-L_D}{\delta_{ss}} = 4L_\delta + \frac{H_\delta}{H_G} L_{\dot{\phi}} \tag{4}$$

The second term on the right-hand side of equation (3) is significant in that it represents the roll-damping contribution of the rollerons to the missile and the pertinent physical quantities upon which it depends. Examination of this term indicates that the rolleron damping contribution is directly proportional to the gyro-wheel angular momentum and the ratio of aileron roll effectiveness L_δ to the aileron hinge-moment parameter H_δ.

Stability-Boundary Charts

Rewriting equations (1) and (2) by using operator notation gives

$$\left(I_X D^2 - L_{\dot{\phi}} D\right) \frac{\phi}{57.3} + \left(-4H_R D^2 - 4H_G D - 4L_\delta\right)\delta = L_D \tag{5}$$

$$\left(H_R D^2 - H_G D\right) \frac{\phi}{57.3} + \left(-I_R D^2 + H_{\dot{\delta}} D + H_\delta\right)\delta = 0 \tag{6}$$

The characteristic equation is

$$a_o D^3 + a_1 D^2 + a_2 D + a_3 = 0 \tag{7}$$

where

$$a_o = I_R I_X - 4H_R^2$$

$$a_1 = - I_X H_{\dot{\delta}} - I_R L_{\dot{\phi}}$$

$$a_2 = 4H_G^2 + H_{\dot{\delta}} L_{\dot{\phi}} - 4H_R L_\delta - I_X H_\delta$$

$$a_3 = H_\delta L_{\dot{\phi}} + 4H_G L_\delta$$

A stable roll system will exist if, and only if, the following relationships between the coefficients of the characteristic equation (7) are satisfied. See reference 2 for a derivation of these conditions.

$$a_o > 0$$

$$a_1 > 0$$

$$a_1 a_2 - a_o a_3 > 0 \quad \text{(Oscillatory stability boundary)}$$

$$a_3 > 0 \quad \text{(Static stability boundary)}$$

The actual stability boundaries are obtained by setting the above expressions equal to zero.

In figures 6 to 11 are shown the stability-boundary plots, based upon the above stability conditions, obtained by using the measured rolleron characteristics and the roll inertia at burnout of models A and B given in table I. Since no experimental data exist at the present time for the aerodynamic characteristics $\left(L_\delta,\ L_{\dot{\phi}},\ \text{and}\ H_\delta\right)$, the charts were calculated with these parameters as the principal variables. Each figure has been plotted with H_δ as the ordinate and L_δ as the abscissa for the estimated minimum and maximum missile roll damping, $L_{\dot{\phi}} = -0.05$ and -5.0 ft-lb/radian/sec and gyro-wheel spin rates of 10,000, 30,000, and 50,000 revolutions per minute. In order to indicate the effect of

control-surface damping, three arbitrary values of $H_{\delta}^{\cdot}$ were used in the calculations, -0.05, -0.10, and -0.25 (for model A only) ft-lb/radian/sec, in addition to the experimentally measured control-surface damping of models A and B. (See table I.) The darkened area in each figure designates the values of H_{δ} and L_{δ} anticipated for the operation of the missile and was estimated from reference 3 and unpublished data. In table II are shown estimated values of $C_{l_{\delta}}$, C_{l_p}, and $C_{h_{\delta}}$ for three Mach numbers. A slight increase in the darkened area defined by this reference and the unpublished data was arbitrarily made to account for unknown factors.

In general, for both models A and B a stable system exists for small values of control-surface damping if the gyro-wheel speed is sufficiently low. As the gyro-wheel speed is increased, the operating region of the missile lies practically within the dynamically unstable region for relatively low values of control-surface damping. For higher values of control-surface damping, stability is achieved on both models at the highest gyro-wheel rates shown. Thus, for a given amount of control-surface damping, there is an ultimate limit of wheel speed corresponding with stability for models A and B. Consequently, the steady-state roll-damping contribution of the rolleron to the missile defined in equation (3) is restricted by dynamic stability considerations.

The oscillatory stability boundaries drawn for the experimentally measured control-surface damping of models A and B are shown in figures 6 to 11 by a solid line. Model A has less than the necessary damping for stability as evidenced by the respective positions of the oscillatory boundary and the operating region. Adequate damping is present in model B since the estimated operating region lies within the stable region defined by the conditions of stability. It should be noted that the position of the static stability boundary is independent of the control-surface damping and that the missile inherent roll damping $L_{\dot{\phi}}$ has only a slight effect on the dynamic roll stability of the rolleron system.

ROLLERON-DAMPER DESIGN

Viscous-Type Damper

Preliminary design of the rolleron damper for model B centered on a viscous type. In order to provide control-surface damping, this device utilized fluid in a gap between a shaft rigidly connected to the wing and the cylindrical rolleron housing. A gap of 0.001 inch, together with the highest viscosity silicone fluid available (10^6 centistokes), provided

a control-surface damping of only -0.06 ft-lb/radian/sec. Misalinement problems associated with the small gap further complicated the use of this device.

Orifice-Type Damper

Final design of the orifice-type rolleron damper for model B is shown in figures 12 and 13. When the rolleron is deflected, fluid damping is obtained by restricting the flow through the two orifices formed by an 0.001-inch gap between the vane shaft rigidly fastened to the wing and the knife edges of the vee-inserts mounted inside the rolleron cylindrical housing. Each orifice had a design area of 0.00162 square inch; however, no rigid control of the tolerances on the machine work for the components was made and it is estimated that actual orifice area plus leakage around the vane and vee-block ends varied the design value by approximately 25 percent. The vane shaft was taper pinned to the wing at both ends and positioning of the rolleron on the shaft was accomplished by means of shims at each end. Leakage was controlled by conventional O-ring seals. A special tool was required for installation of the vee-inserts to maintain the proper alinement.

Selection of the viscosity of the damper fluid for this unit was made on the basis of eliminating any spring effects due to the flexibility of the vane shaft, since the rolleron hinge-moment parameter H_δ is the sum of the aerodynamic and damper internal spring force. In order to simplify the rolleron installation procedure, the viscosity of the damper fluid was standardized for the four units. Other tests indicated that the machine tolerances employed were adequate for the range of viscosities presently available in the silicone fluids.

Experimental Technique and Measurements

The effectiveness of the dampers was ascertained by experimental measurement. The laboratory test rig used is shown in figure 14. The experimental technique was based on the following assumptions:

(1) The rolleron motion was confined to one-degree-of-freedom rotation about the hinge line.

(2) The rolleron, when spring restrained and damped, can be represented by a linear second-order system.

The values of $H_{\dot{\delta}}$ were calculated from the relationship $H_{\dot{\delta}} = 2\zeta\sqrt{\frac{H_\delta}{I_R}}$ where $2\sqrt{\frac{H_\delta}{I_R}}$ equaled 0.25 for all the test runs. The damping ratio ζ

was obtained by comparison of the system transient response with typical response curves of second-order systems to step-function disturbances. Admittedly, the final damper designed for model B is not a linear device; however, bench tests appear to validate the use of linear theory for design purposes.

On the basis of laboratory tests, silicone fluid with a viscosity of 20,000 centistokes was selected as approaching the damping specified. Transient responses of the rollerons installed on model B, subsequent to an initial deflection of 10°, are shown in figure 15. The average value of $H_{\delta} = -0.21$ ft-lb/radian/sec for the four rollerons meets the damping requirements. Rolleron number 4 exhibited the least damping, probably because of larger tolerances in construction; however, the shape of the transient response is an excellent illustration to substantiate the linear-second-order-system assumption. The response of rolleron number 1 implies a higher order response and is attributed to closer construction tolerances. Further tests with higher viscosity fluids aggravated this type of response, which was apparently caused by a second spring constant introduced by a lack of rigidity of the vane shaft. Rollerons 2 and 3 exhibited a damping ratio greater than unity.

Experience with the orifice damper showed no loss of effectiveness due to leakage over a period of more than two months, when the rollerons remained locked in the streamline position. Tests indicated that the rigidity of the vane shaft should be increased for future use of this device if greater damping is desired.

Measurements on the rollerons of model A, which did not have rolleron dampers, obtained by using the technique described above indicated that a control-surface damping of -0.0036 ft-lb/radian/sec could be used to represent the hinge-pin friction for purposes of roll-system stability calculations.

MODEL FLIGHT-TEST TECHNIQUE

Instrumentation

Model A was equipped with a four-channel telemeter which transmitted a continuous record of normal and transverse acceleration, rate of yaw, and rate of roll. Model B was equipped with a five-channel telemeter which transmitted a continuous record of normal and transverse acceleration, rate of yaw, rate of roll, and gyro-wheel speed.

The measured response of the instrument rate gyro used to measure rate of roll and rate of yaw is given below.

	Undamped natural frequency, cps		Critical damping, percent	
	Model A	Model B	Model A	Model B
Rate of yaw	50	75	70	45
Rate of roll	50	75	70	52

In general, the accuracy of the telemetered data is approximately 2 to 5 percent of full scale if the frequencies encountered do not exceed the instrument undamped natural frequency.

The model trajectory was determined by a modified SCR 584 radar tracking unit. Model velocity was obtained from a CW Doppler velocimeter. A radiosonde released at the time of flight measured atmospheric temperature and pressure through the altitude range traversed by the models.

Free-Flight and Launching Conditions

The models were boosted to supersonic velocities by a solid-propellant rocket motor which delivered approximately 6,000 pounds of thrust for 3.0 seconds. A sustainer, made as an integral part of the models, delivered approximately 3,000 pounds of thrust for 2.6 seconds and propelled model A and model B to peak Mach numbers of 2.34 and 2.37, respectively. Presented in figures 16 and 17 are the flight time histories of velocity, Mach number, and dynamic pressure for both models A and B. Reynolds number based on body length is shown plotted against Mach number in figure 18.

Prior to the flight test of the models, the gyro wheel of the rollerons on both models was given an initial rotational speed. This initial speed given the gyro wheels tended to overcome the starting inertia and friction of the gyro wheel and thus simulated more accurately an actual operational missile air launch. The initial rotational speed of the rollerons was accomplished by applying a source of air to each of the rollerons while the model was on the launcher and allowing this air

supply to turn the rollerons until the model had moved clear of the launcher. Presented in figure 19 is a photograph of model A and booster on the launcher showing the arrangement used to apply the air to the rollerons prior to firing. The launching angle was 60° with respect to the horizontal. Gyro-wheel speed of model B is shown in figure 17. Firings of the models were conducted at the Langley Pilotless Aircraft Research Station at Wallops Island, Va.

RESULTS AND DISCUSSION

Roll Dynamic Stability

The roll stability of the free-flight test models A and B is clearly demonstrated by the time history of the model roll velocity shown in selected portions of the continuous-type telemeter record reproduced in figures 20 and 21. In the uncalibrated telemeter-record reproductions, the running variable, in all cases, is time and the uncalibrated deflection from an arbitrary base line represents the relative magnitude of the measured quantities indicated. No programmed model disturbances were generated during coasting; therefore, rolling moments applied to the missile were caused by the aerodynamic out-of-trim condition due to model construction asymmetries, gusts, and inertia coupling from other missile modes of motion. These disturbances were apparently sufficient, since, as predicted, model A did reveal an inherent dynamic instability in the form of a divergent oscillatory roll oscillation at $M = 2.07$. The divergence progressed for approximately 0.4 second and was immediately followed by a self-sustained oscillation, characterized by two predominant frequencies, which were present for the remainder of the model flight. Envelope half-amplitude and frequency plots of the self-sustained oscillation (lower frequency mode only) are shown in figure 22 for model A. In general, both the frequency and oscillation amplitude decreased with decreasing Mach number. By integration of the roll-velocity time history, the roll-oscillation amplitude was shown to be $\pm 2.5^{\circ}$ at $M = 1.6$ and $\pm 5.0^{\circ}$ at $M = 0.6$. No corrections to the roll-velocity record to account for the band-pass characteristics of the instrumentation were made because the frequencies encountered were well below the undamped natural frequency of the roll-velocity instrument.

Model B was dynamically stable in roll throughout the flight as illustrated in figure 21. Since the primary difference between models A and B was the amount of control-surface damping, the complete elimination of any undesirable unstable oscillatory modes can only be attributed to this cause. Reexamination of the stability boundary plots for models A and B (figs. 6 to 11) reveals the possibility of other system modifications which would have achieved stability. For example, if the operating region could have been rotated in a counterclockwise direction by either an

increase in H_δ or a decrease in L_δ, then stable operation would have resulted. However, by equation (3), it is seen that a decrease in the missile roll-damping contribution would have been produced by either of these system modifications. Obviously, the optimum design is that which gives the greatest missile roll damping without enticing a dynamic roll instability by operation too close to an oscillatory stability boundary. For the missile and control-surface configuration investigated, the greater the control-surface damping, the greater the gyro-wheel angular momentum permissible consistent with stability. Since the rolleron-to-missile roll-damping contribution was previously shown to be directly proportional to the gyro-wheel angular momentum, the addition of control-surface damping was the most desirable and practical rolleron-system modification.

Rolleron Roll-Damping Effectiveness

The mean roll velocities of models A and B are plotted against Mach number in figure 23. During the self-sustained roll oscillation of model A, the mean roll velocity is illustrated since this is the effective rate which eventually produces rotation of the missile from some arbitrary roll reference position. The roll damping of the missile-rolleron system cannot be measured with the instrumentation employed because the applied rolling moment is unknown. Nevertheless, these two models could very well be considered to represent typical production missiles and since the steady-state roll rate is within the assumed roll specifications, the rollerons apparently did provide satisfactory roll damping. Theoretical estimates of the missile-rolleron combination roll damping indicate a fivefold to tenfold improvement over the inherent missile aerodynamic roll damping without rollerons.

Model A exhibited a significant increase in subsonic roll rate which was not present in model B. The reason for this effect is unknown; however, roll velocities on the order of 150 degrees per second to 200 degrees per second are not unusually high for missiles of this type on which no quality control of the minimization of out-of-trim rolling moment during model construction was undertaken. Because of this situation and since the gyro-wheel speed of model A was not measured, a comparison of the roll damping of models A and B on the basis of the measured roll rate is not valid.

Rolleron Gyro-Wheel Speed

The gyro-wheel angular velocity is plotted against Mach number for model B in figure 23. The magnitude obtained on the flight test was of the order anticipated and did not exceed the maximum design estimates. A peak angular rate of approximately 45,000 revolutions per minute which corresponds to a peripheral gyro-wheel velocity of 590 feet per second

resulted. No meaningful correlation of the gyro-wheel speed with missile forward velocity is possible which would allow a designer to predict transient (as in this flight) or steady-state wheel rates under a different set of flight and launching conditions. This is primarily a consequence of the unavoidable and somewhat complex interdependence of gyro-wheel aerodynamic and bearing friction torques as well as initial conditions on the missile forward velocity and gyro-wheel angular speed.

Rolleron Longitudinal Characteristics

Qualitative information was obtained on the longitudinal effects of the rollerons from the normal- and transverse-acceleration time histories. Model A exhibited a somewhat spasmodic variation of normal and transverse acceleration with time during the self-sustained roll oscillation, which was at all times less than 2g. (See fig. 20.) A pitch frequency that was approximately equal to the higher of the two predominant roll frequencies discernible was detectable on the record. Apparently, coupling between the roll and pitch modes was in evidence. Model B was subjected to a slight disturbance near sustainer-rocket-motor burnout. (See fig. 24.) The source of this disturbance is not known but it may have been produced by uneven rocket-propellant burning. Two well-defined pitch frequencies are present on the record, the maximum normal acceleration being less than 6g. Both oscillatory modes are stable and possess adequate damping. A theoretical longitudinal-stability study of free-floating pitch-control surfaces, reported in reference 4, predicts the presence of these two oscillatory modes. Although the arrangement of the control surfaces utilized and the airframe investigated in reference 4 are not identical to models A and B, the results obtained therein should be indicative since the rolleron gyro wheels remain inactive to pitching motion for relatively small control-surface deflections.

CONCLUDING REMARKS

Rollerons furnished effective roll-rate stabilization on the two research configurations tested. The measured mean roll rate on both models was less than 1 radian per second and within the assumed roll specifications throughout the assumed operating flight conditions of the missile. An undesirably high-frequency (30 cps) self-sustained roll oscillation, due primarily to a dynamic roll instability which was predictable on the basis of linear theory, was present on the first flight-test model. This oscillation was eliminated on the second model flown by only the introduction of damping about the hinge line of each rolleron control surface. The addition of control-surface damping not only improved the roll characteristics but also apparently prevented the occurrence of continuous

high-frequency pitching oscillations, which were present during the self-sustained roll oscillation experienced on the model tested without dampers.

System modifications, other than the control-surface damping investigated herein, might have eliminated the objectionable high-frequency self-sustained roll oscillation but may have resulted in smaller steady-state roll damping of the overall missile-rolleron roll-rate stabilization system. Further research would be necessary to establish the advantages and suitability of other modifications. The applicability of rollerons to other similar missile configurations as a means of improving the inherent roll damping could be ascertained, with a fair degree of reliability, by the stability-analysis methods employed herein for the detection and suppression of an undesirable dynamic roll instability.

Langley Aeronautical Laboratory,
National Advisory Committee for Aeronautics,
Langley Field, Va., March 18, 1955.

REFERENCES

1. LaBerge, Walter B., and Drinkwater, W. Dale: Preliminary Evaluation of a Simplified Roll-Rate Stabilization System. NAVORD Rep. 1269 (NOTS 339), U. S. Naval Ord. Test Station (Inyokern, Calif.), Jan. 8, 1951.

2. Routh, Edward John: Dynamics of a System of Rigid Bodies. Part II. Sixth ed., rev. and enl., Macmillan and Co., Ltd., 1905, pp. 223-230.

3. Tucker, Warren A., and Nelson, Robert L.: Theoretical Characteristics in Supersonic Flow of Constant-Chord Partial-Span Control Surfaces on Rectangular Wings Having Finite Thickness. NACA TN 1708, 1948.

4. Curfman, Howard J., Jr., Strass, H. Kurt, and Crane, Harold L.: Investigations Toward Simplification of Missile Control Systems. NACA RM L53I21a, 1953.

TABLE I

MASS AND INERTIA CHARACTERISTICS

(a) Rocket models

	Model A	Model B
Take-off weight, lb	148.5	149.2
Burnout weight, lb	105.0	108.5
Take-off mass, slugs	4.61	4.64
Burnout mass, slugs	3.26	3.37
Take-off center-of-gravity location (measured from nose), in.	55.63	56.72
Burnout center-of-gravity location (measured from nose), in.	49.75	51.30
I_Y (burnout), slug-ft^2	31.08	30.17
I_X (burnout), slug-ft^2	0.30	0.30

(b) Rollerons

	Model A	Model B
I_R, slug-ft^2	0.000705	0.000849
I_G, slug-ft^2	0.000198	0.000205
m, slug	0.0310	0.0297
$\bar{l}$, ft	0.775	0.775
$\bar{d}$, ft	0.129	0.148
$H_{\dot{\delta}_{av}}$, ft-lb/radian/sec	-0.0036	-0.21

TABLE II

ESTIMATED AERODYNAMIC COEFFICIENTS OF ROCKET MODELS

M	C_{l_δ}	C_{l_p}	C_{h_δ}
1.2	0.74	-6.73	-0.14
1.6	.53	-6.61	-.31
2.0	.41	-5.66	-.27

CONFIDENTIAL

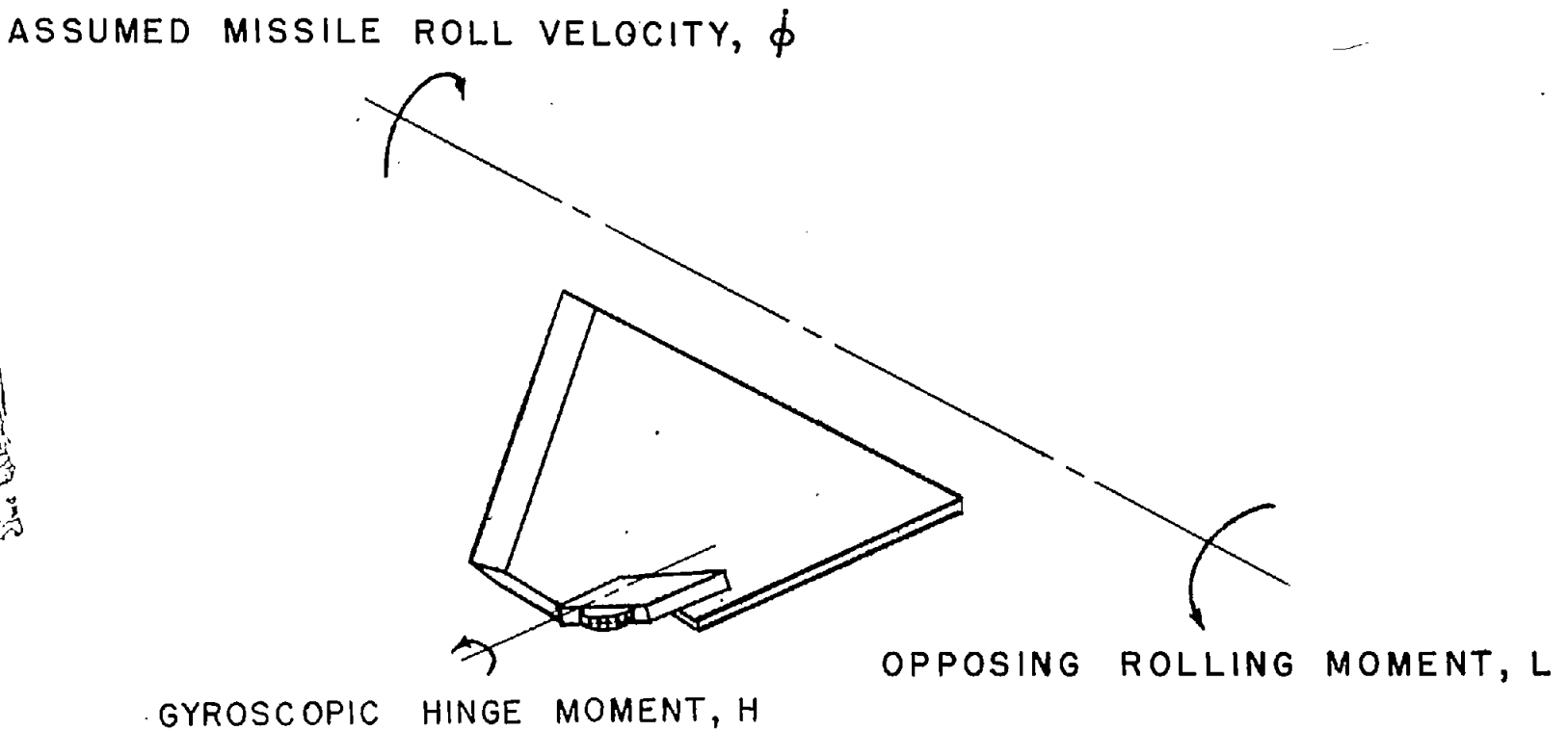

Figure 1.- Rolleron operating principle.

CONFIDENTIAL

CONFIDENTIAL

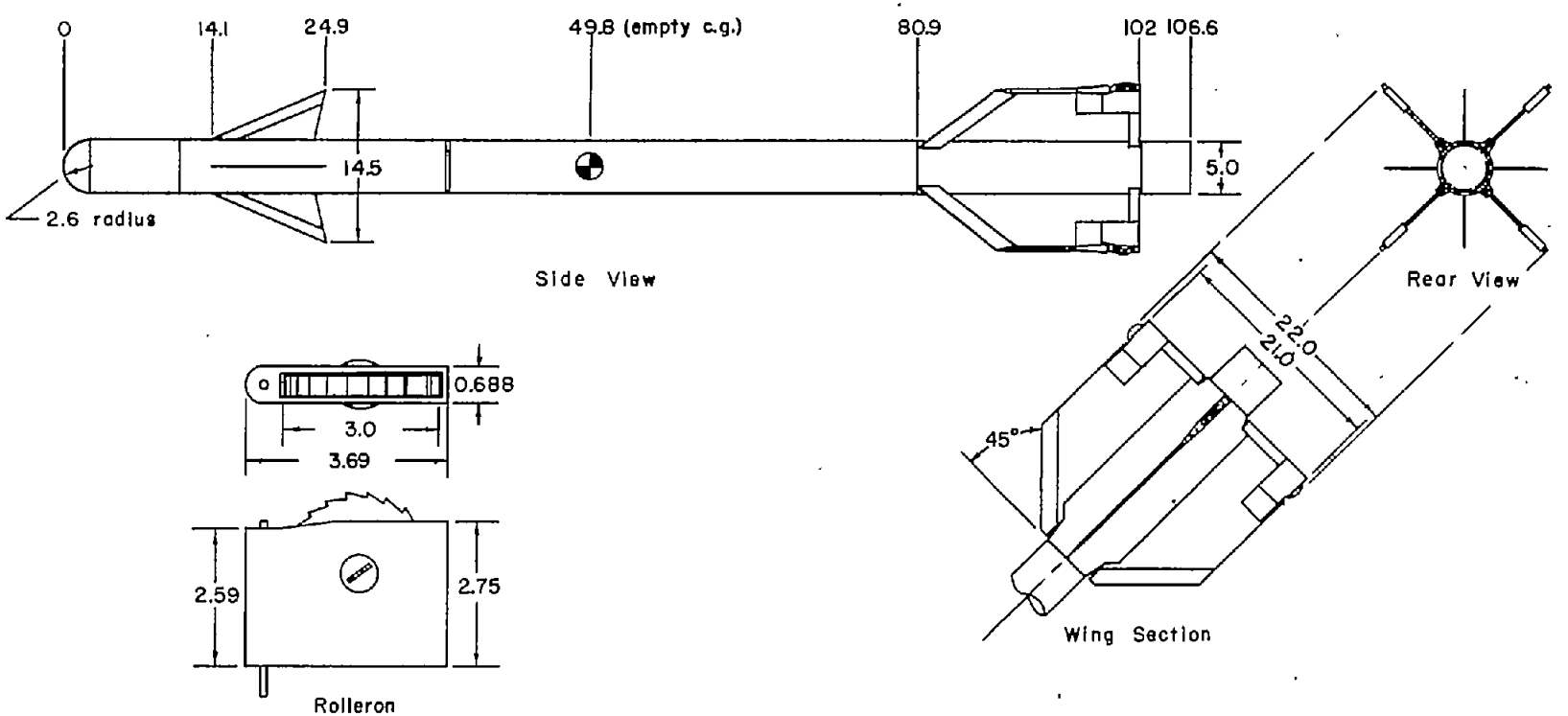

(a) Model A.

Figure 2.- General arrangement of rocket models and rollerons. All dimensions are in inches.

CONFIDENTIAL

CONFIDENTIAL

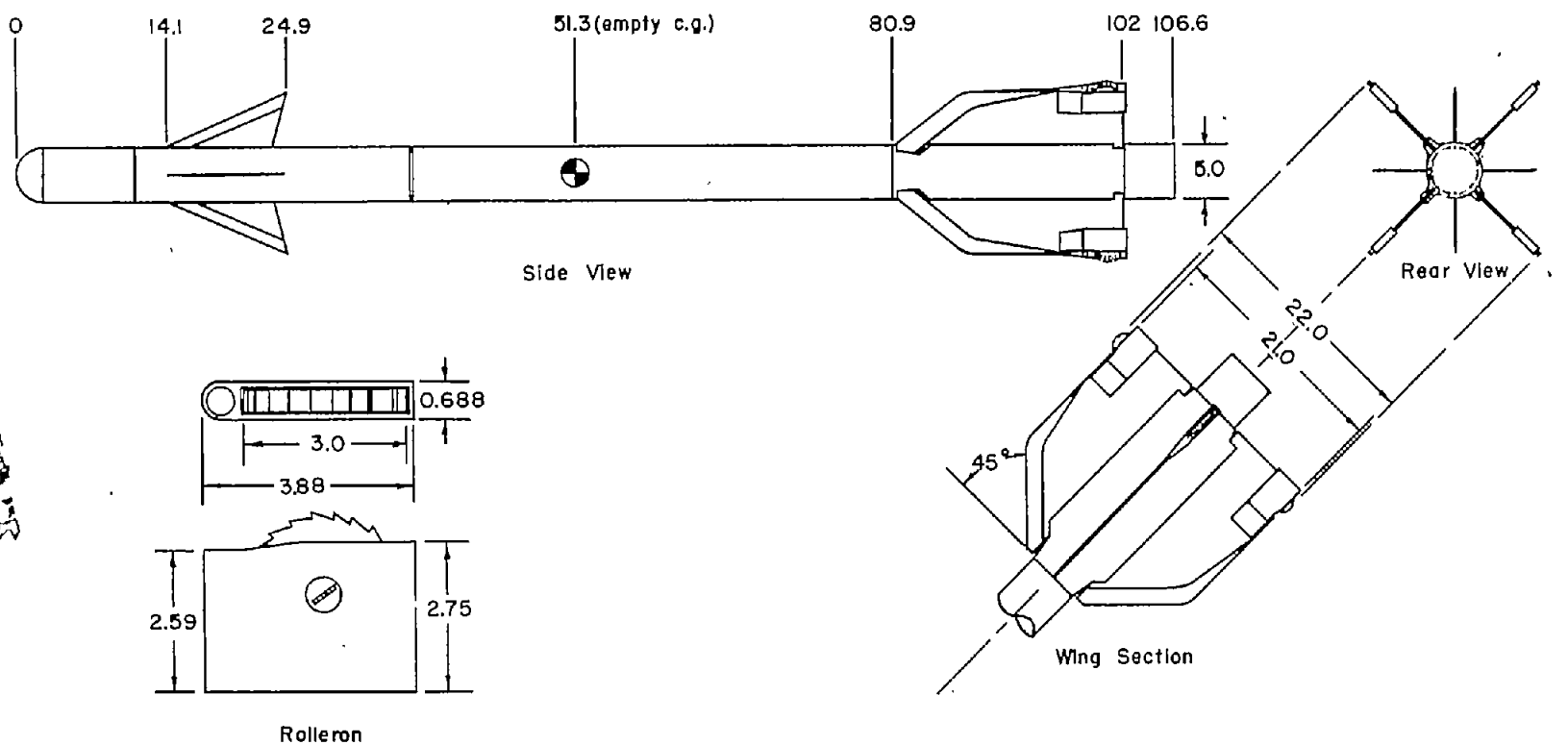

(b) Model B.

Figure 2.- Concluded.

CONFIDENTIAL

CONFIDENTIAL

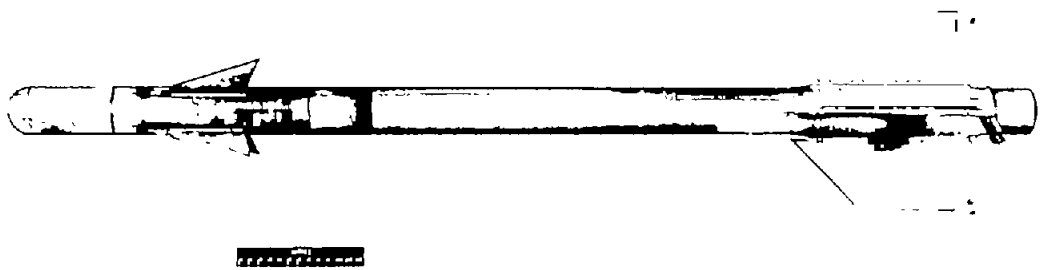

Side view

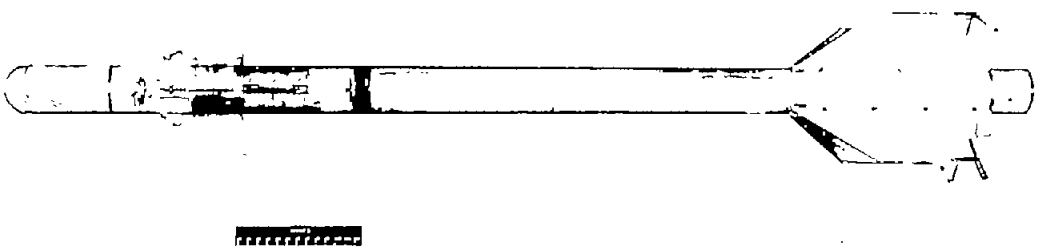

Model rotated 45°

(a) Model A.

L-87910

Figure 3.- Photographs of rocket models with rollerons.

CONFIDENTIAL

CONFIDENTIAL

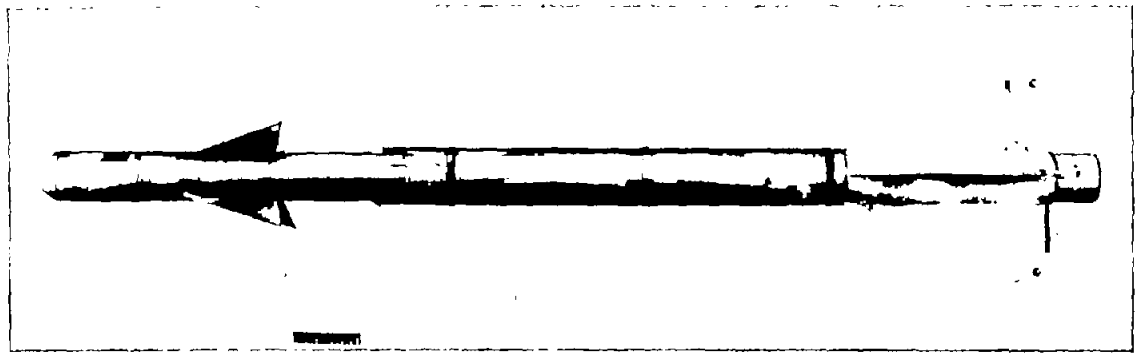

Side view

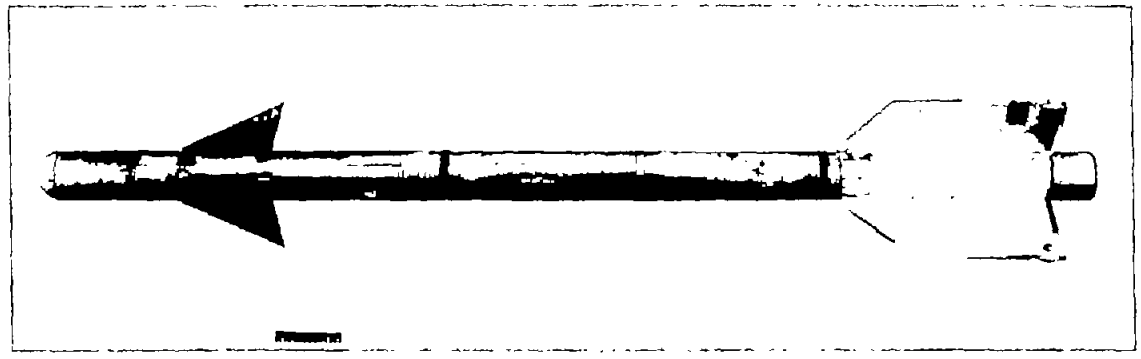

Model rotated 45°

(b) Model B.

L-87909

Figure 3.- Concluded.

CONFIDENTIAL

CONFIDENTIAL

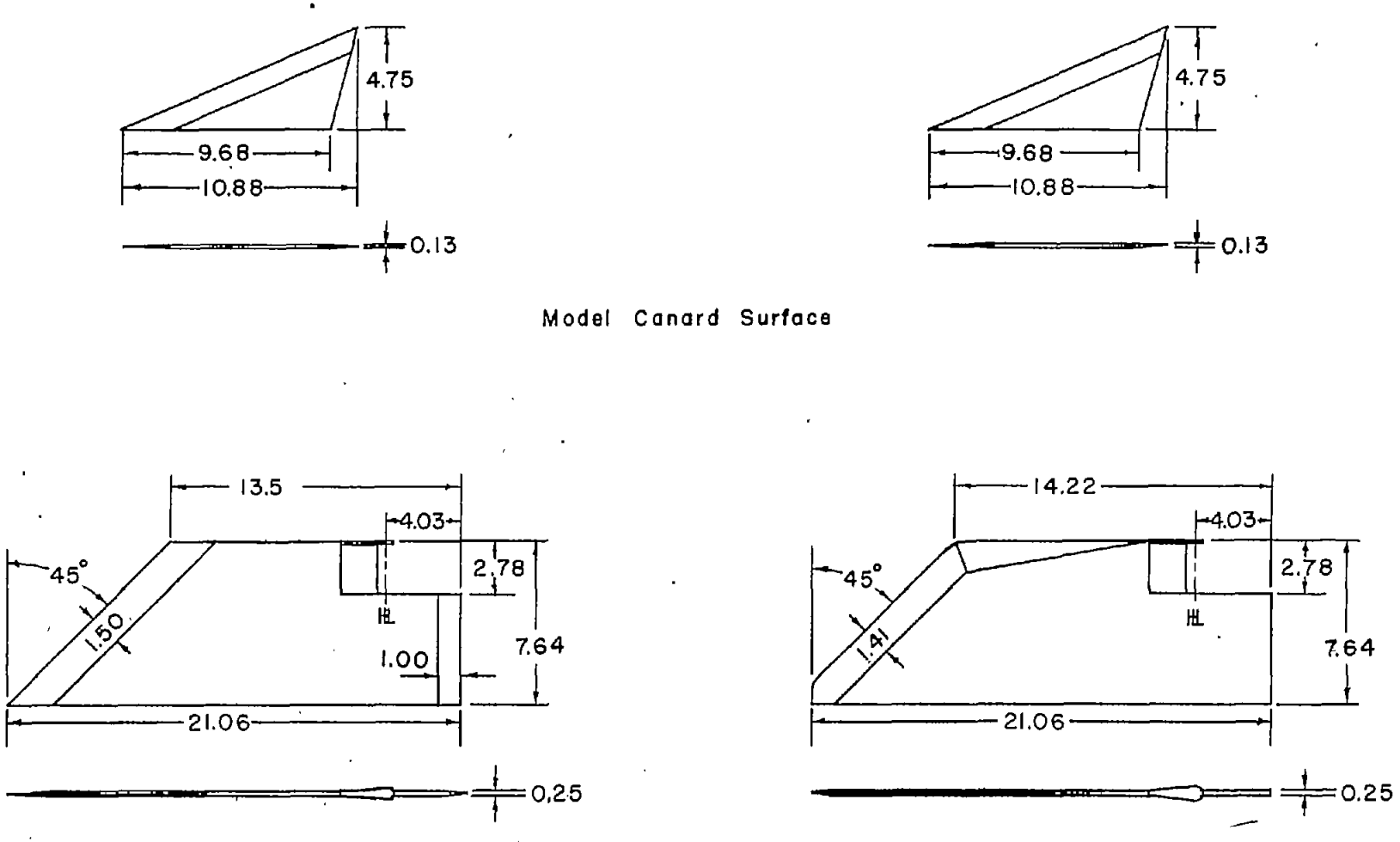

(a) Model A. (b) Model B.

Figure 4.- Sketch of canards and wing surfaces without rollerons for models A and B. All dimensions are in inches.

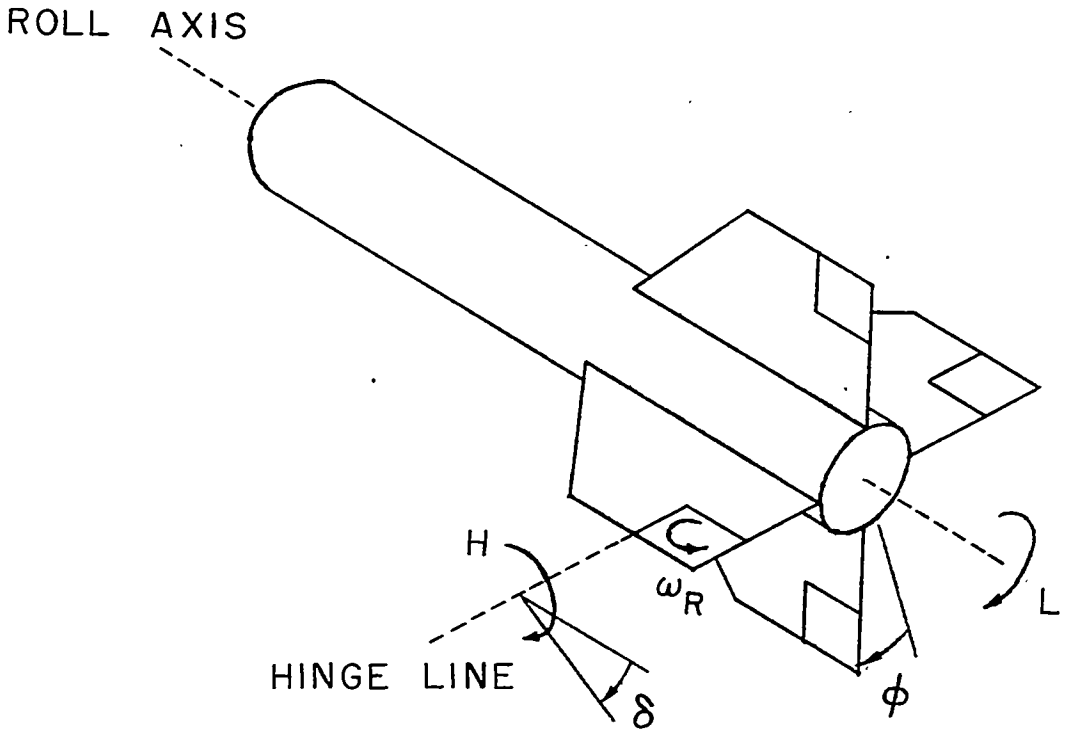

Figure 5.- Sign convention indicating positive directions of moments and angles.

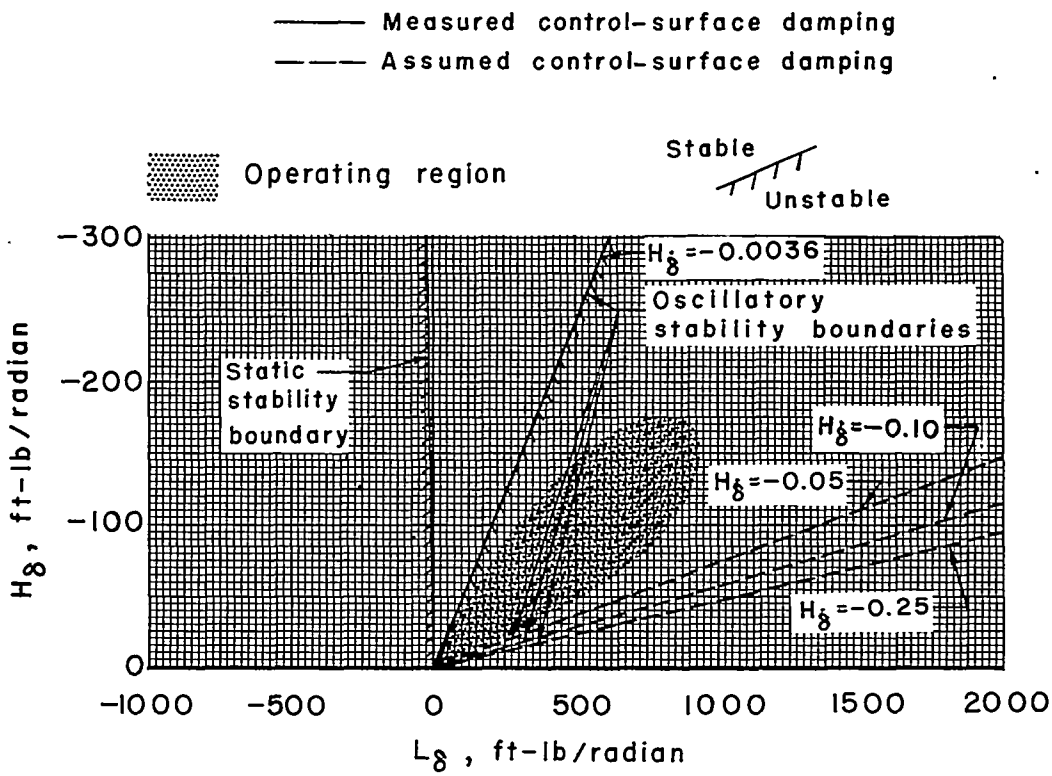

(a) $L_{\dot{\phi}}$ = -0.05 ft-lb/radian/sec.

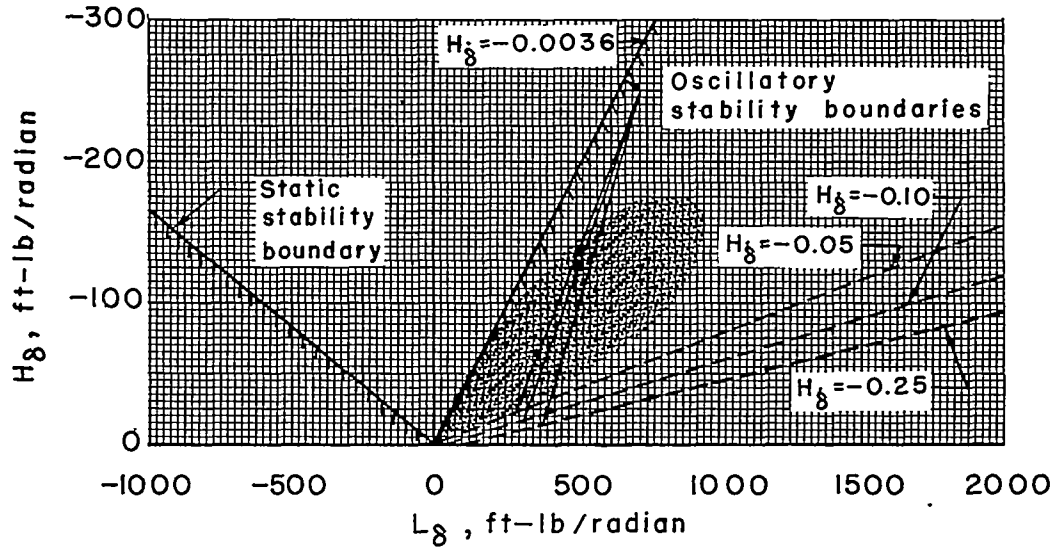

(b) $L_{\dot{\phi}}$ = -5.0 ft-lb/radian/sec.

Figure 6.- Stability-boundary plots showing the effect of control-surface and missile-roll damping for model A at a gyro-wheel speed of 10,000 revolutions per minute.

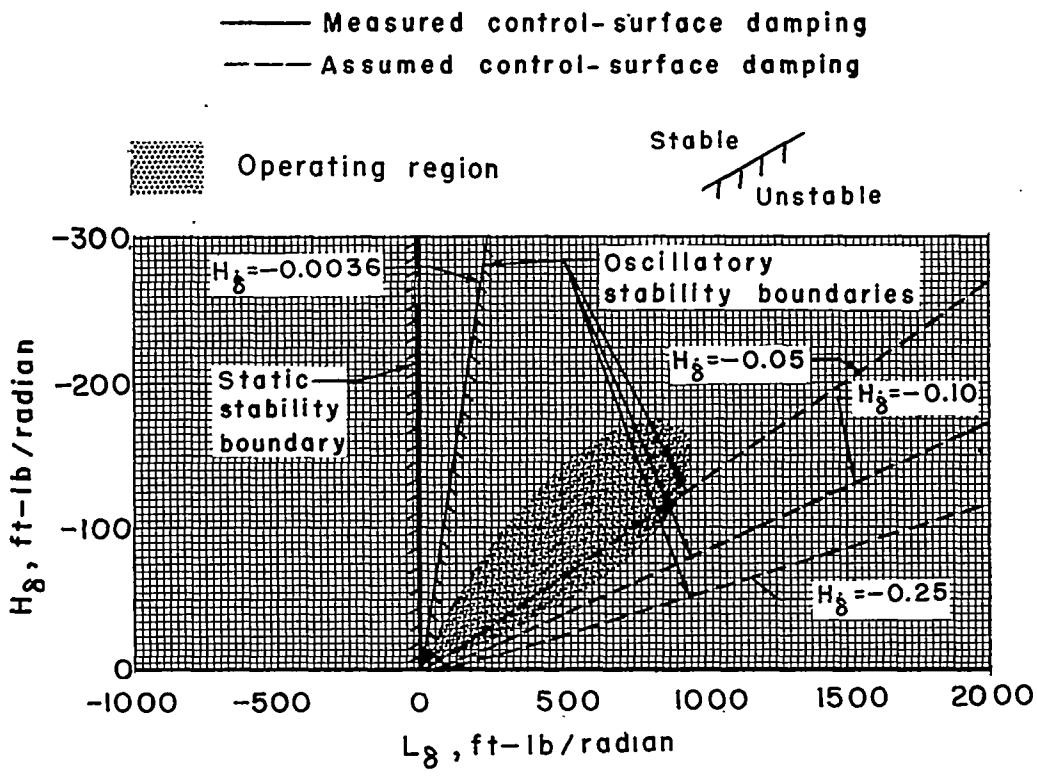

(a) $L_{\dot{\phi}}$ = -0.05 ft-lb/radian/sec.

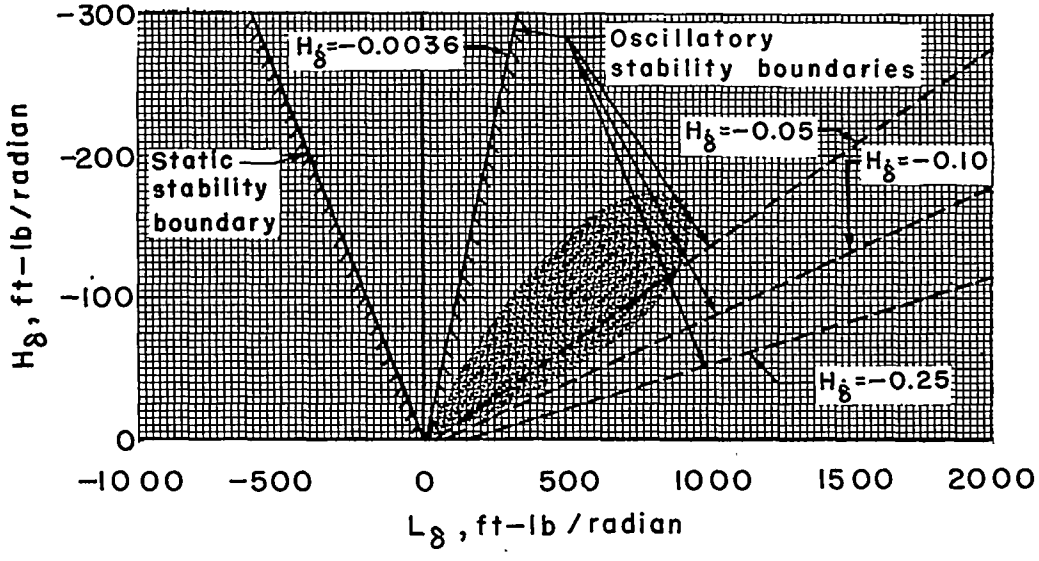

(b) $L_{\dot{\phi}}$ = -5.0 ft-lb/radian/sec.

Figure 7.- Stability-boundary plots showing the effect of control-surface and missile-roll damping for model A at a gyro-wheel speed of 30,000 revolutions per minute.

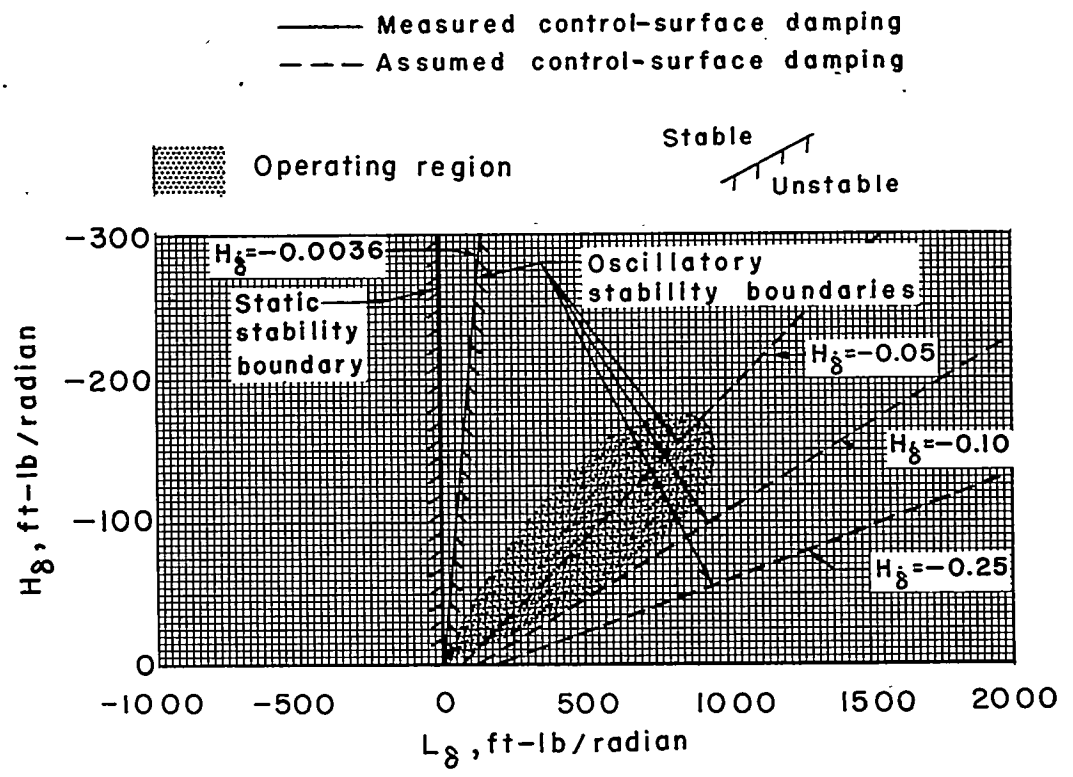

(a) $L_{\dot{\phi}}$ = -0.05 ft-lb/radian/sec.

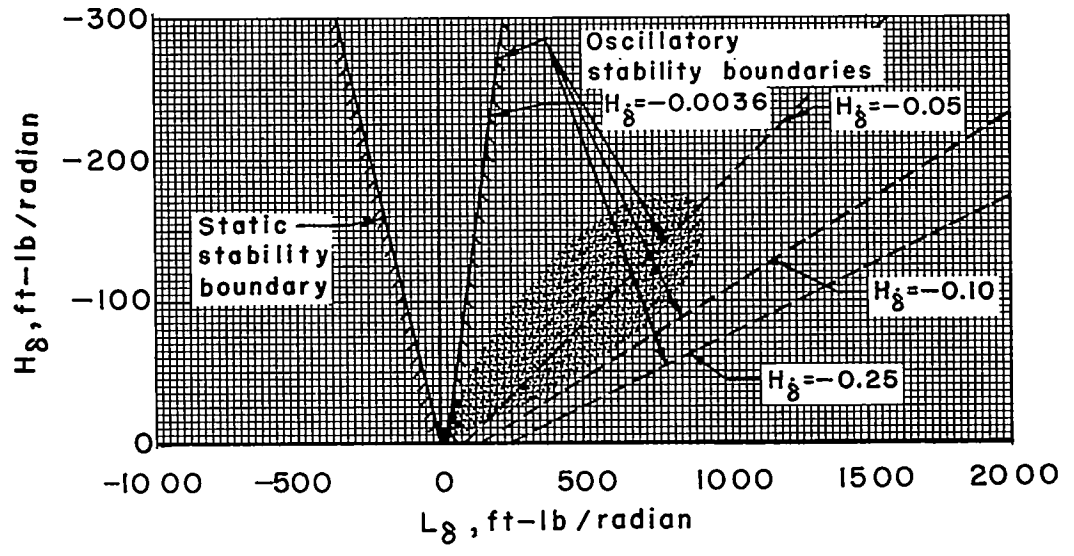

(b) $L_{\dot{\phi}}$ = -5.0 ft-lb/radian/sec.

Figure 8.- Stability-boundary plots showing the effect of control-surface and missile-roll damping for model A at a gyro-wheel speed of 50,000 revolutions per minute.

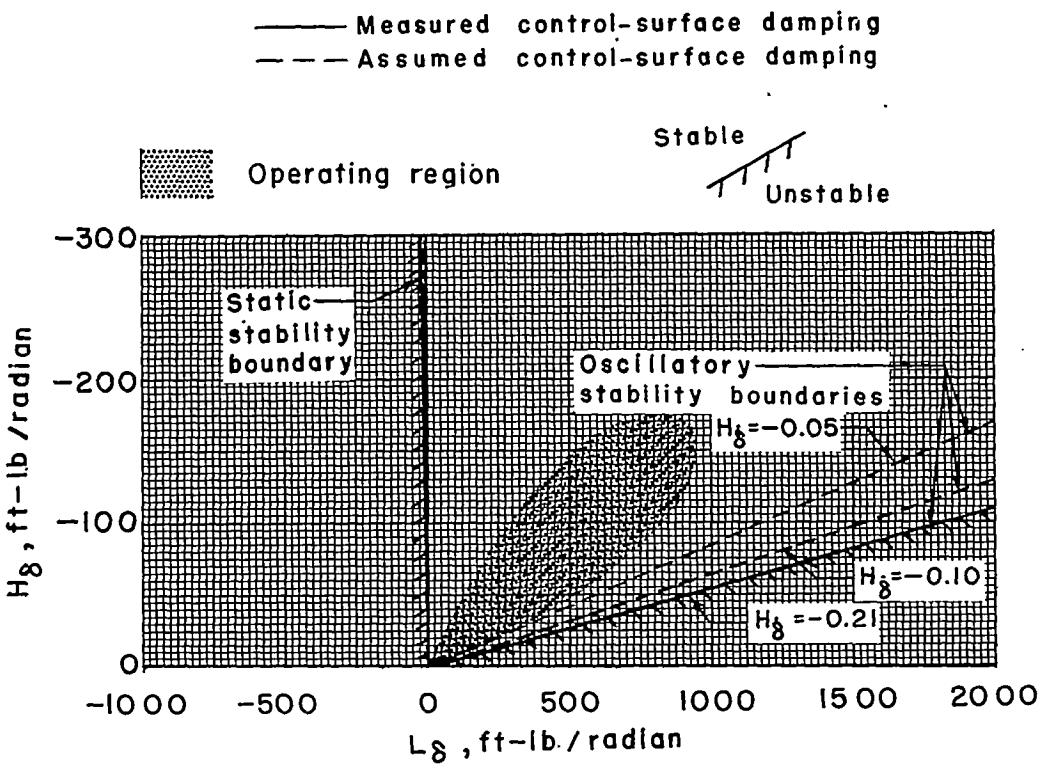

(a) $L_{\dot{\phi}}$ = -0.05 ft-lb/radian/sec.

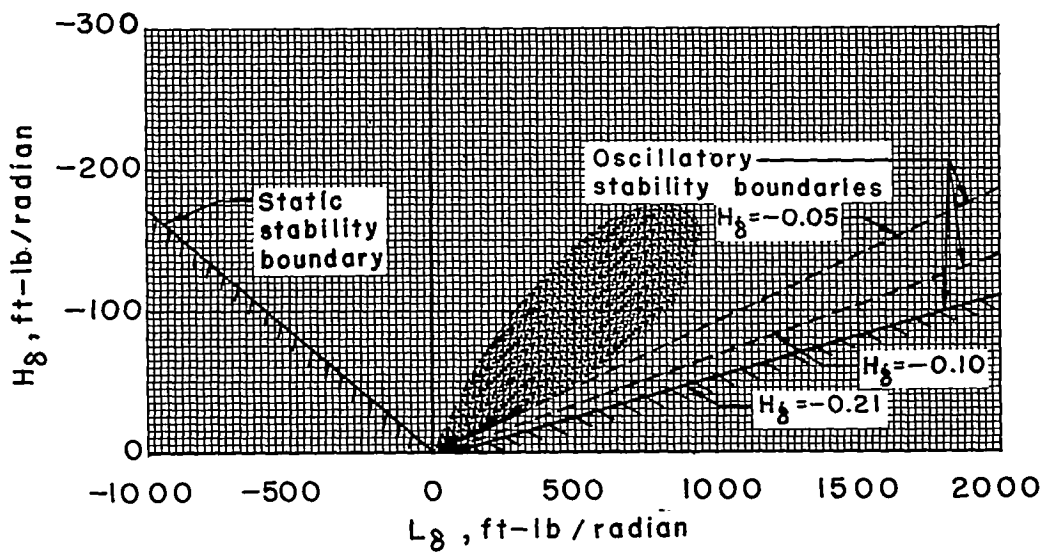

(b) $L_{\dot{\phi}}$ = -5.0 ft-lb/radian/sec.

Figure 9.- Stability-boundary plots showing the effect of control-surface and missile-roll damping for model B at a gyro-wheel speed of 10,000 revolutions per minute.

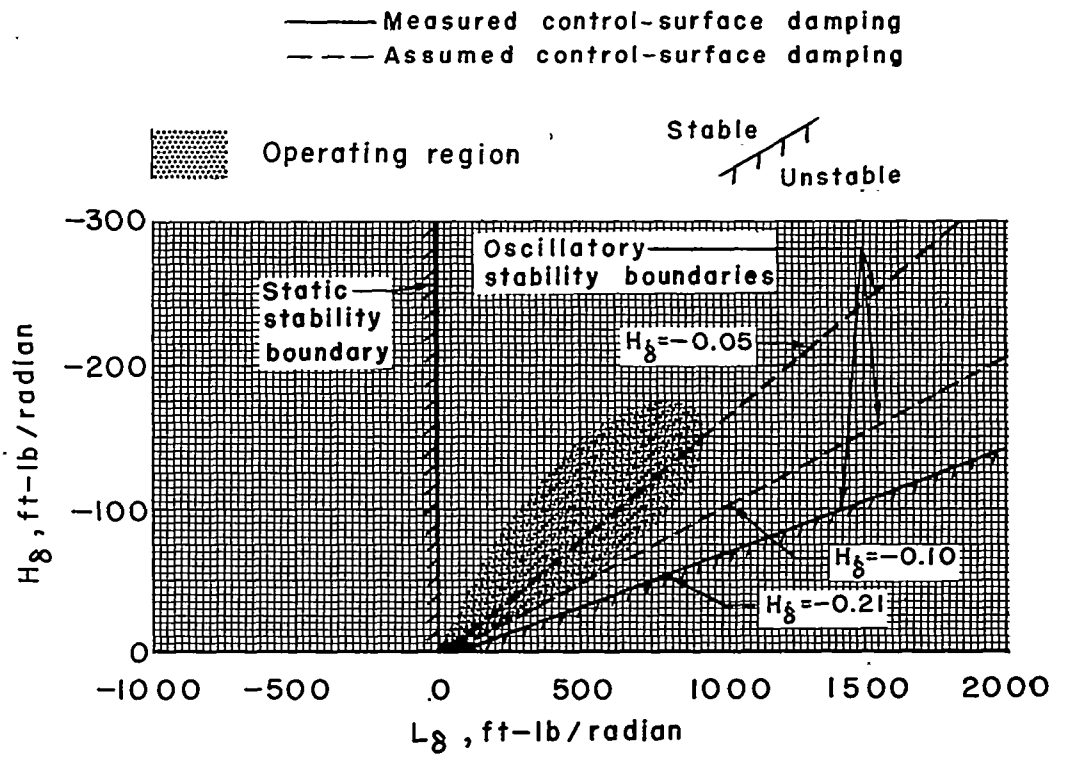

(a) $L_{\dot{\phi}}$ = -0.05 ft-lb/radian/sec.

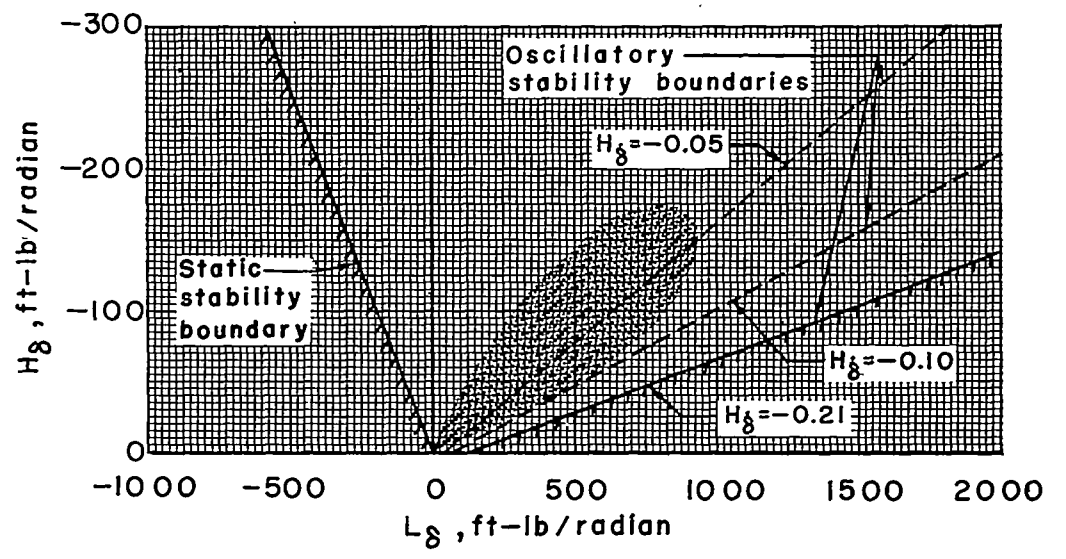

(b) $L_{\dot{\phi}}$ = -5.0 ft-lb/radian/sec.

Figure 10.- Stability-boundary plots showing the effect of control-surface and missile-roll damping for model B at a gyro-wheel speed of 30,000 revolutions per minute.

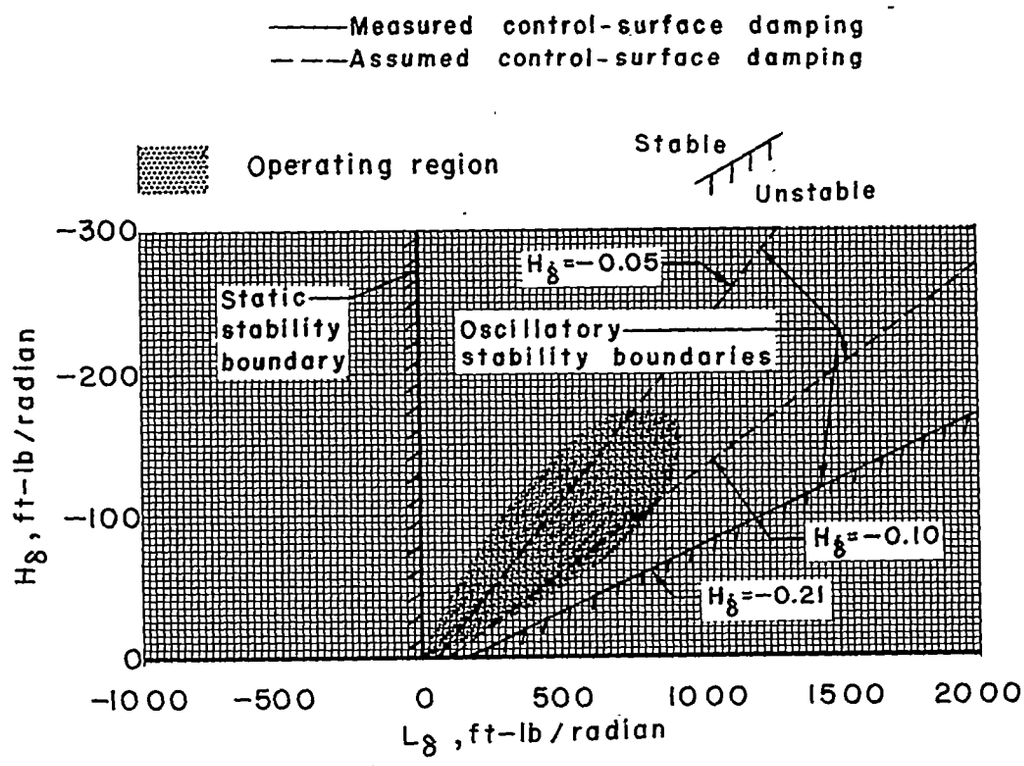

(a) $L_{\dot{\phi}}$ = -0.05 ft-lb/radian/sec.

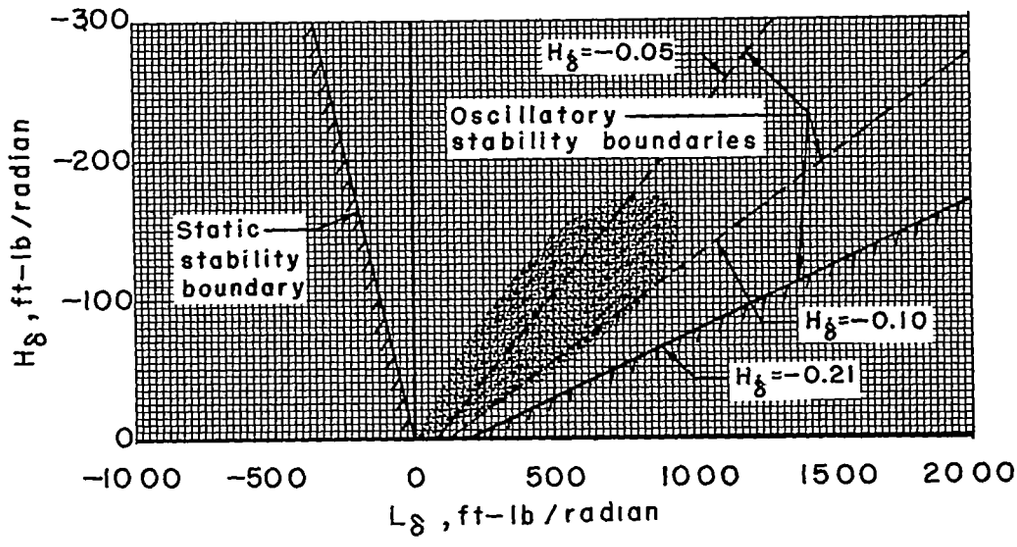

(b) $L_{\dot{\phi}}$ = -5.0 ft-lb/radian/sec.

Figure 11.- Stability-boundary plots showing the effect of control-surface and missile-roll damping for model B at a gyro-wheel speed of 50,000 revolutions per minute.

CONFIDENTIAL

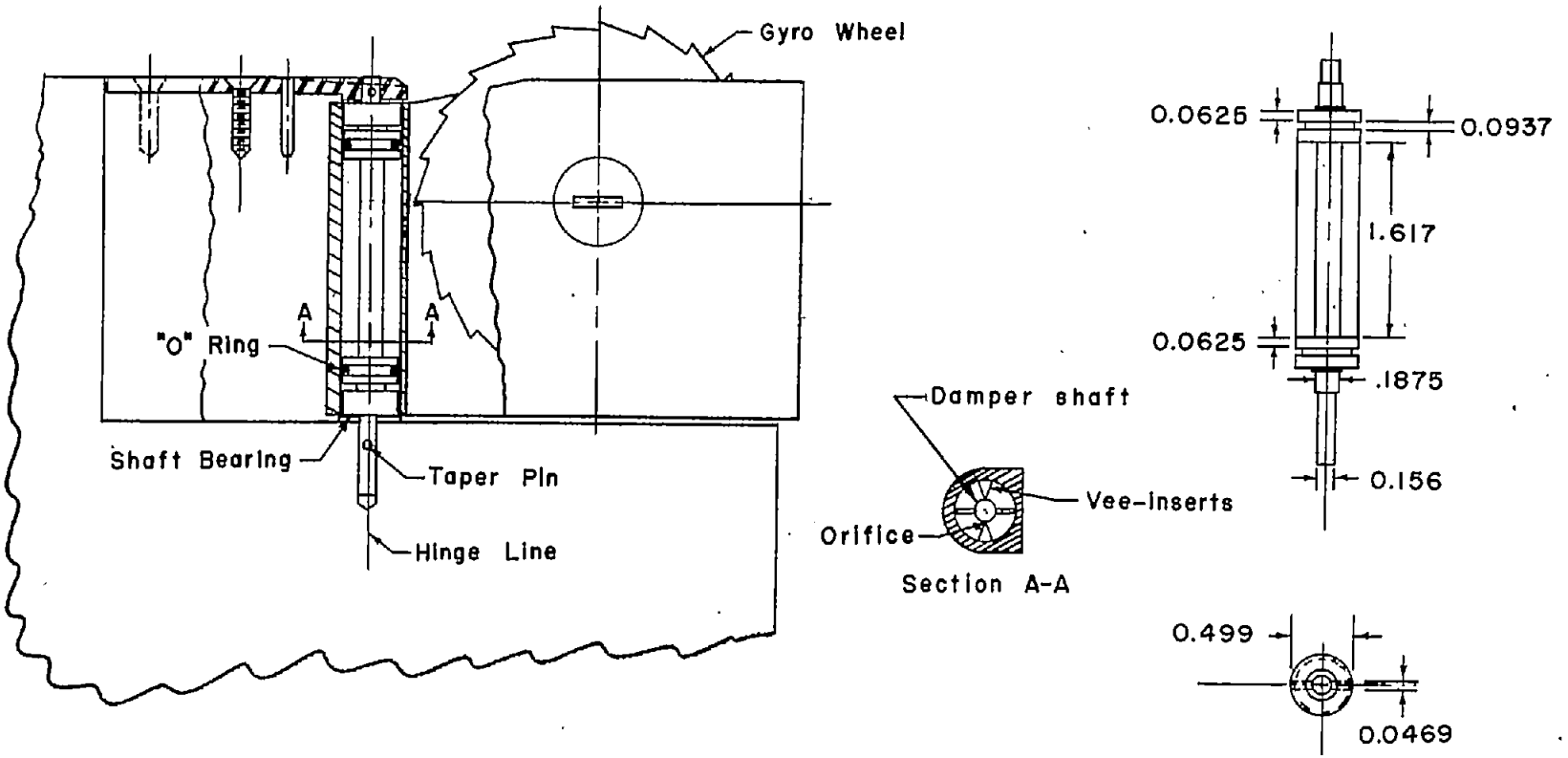

Cutaway View of Rolleron Damper

Rolleron Damper Shaft

Figure 12.- Sketch of rolleron orifice damper for model B.
All dimensions are in inches.

CONFIDENTIAL

CONFIDENTIAL

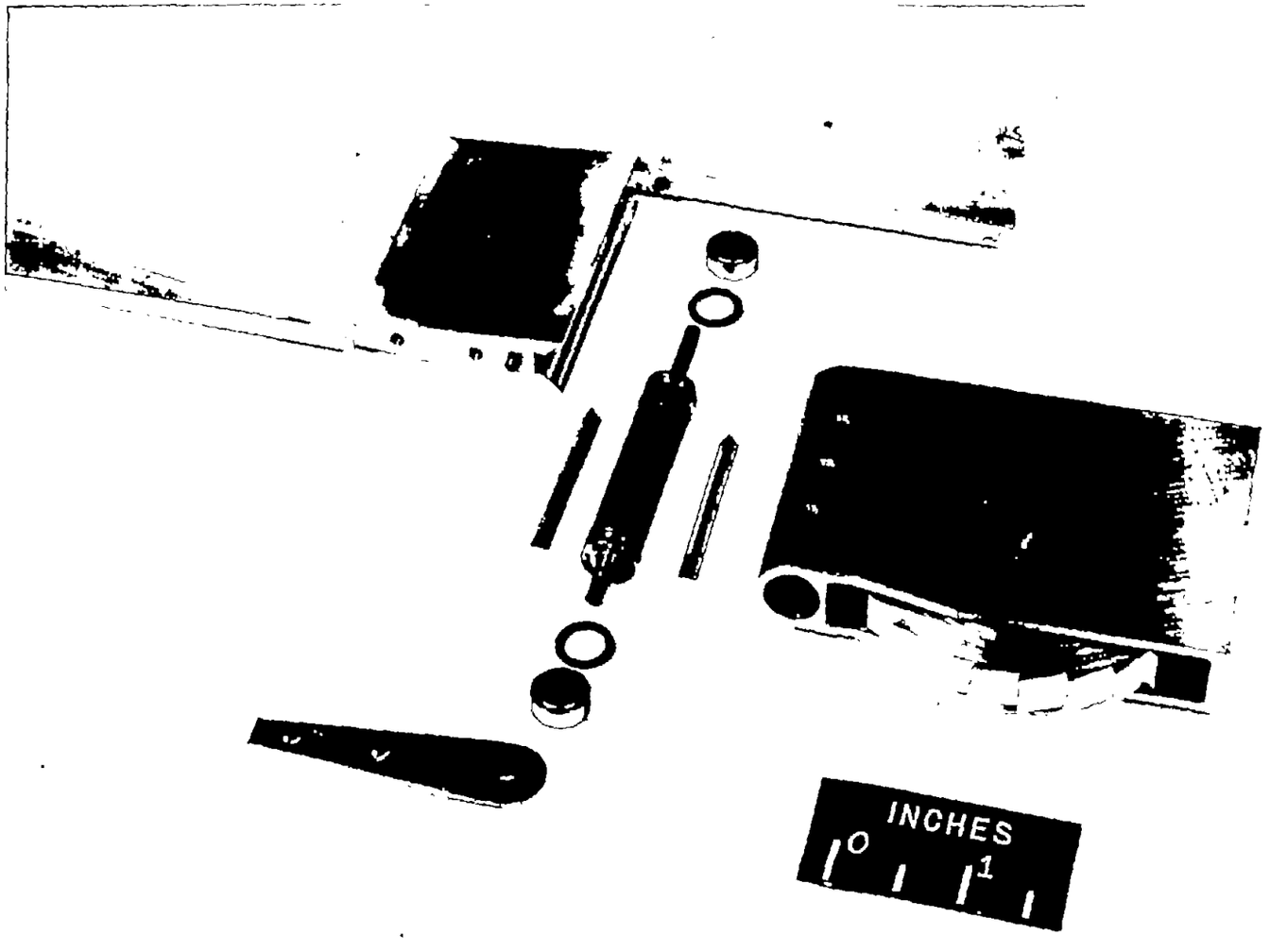

L-85386

Figure 13.- Photograph of orifice damper for model B.

CONFIDENTIAL

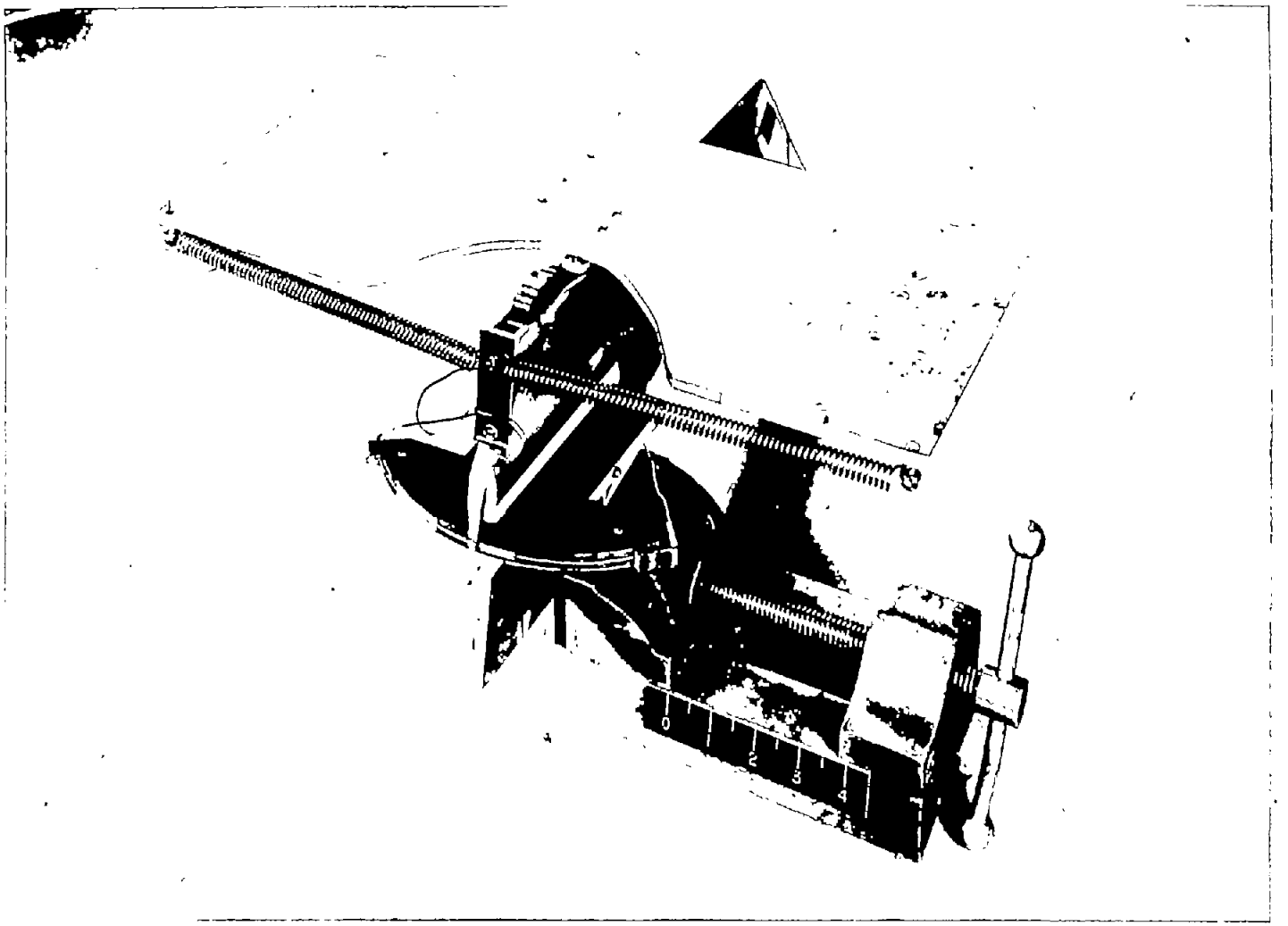

L-82749

Figure 14.- Photograph of laboratory bench test rig used for measurement of control-surface damping.

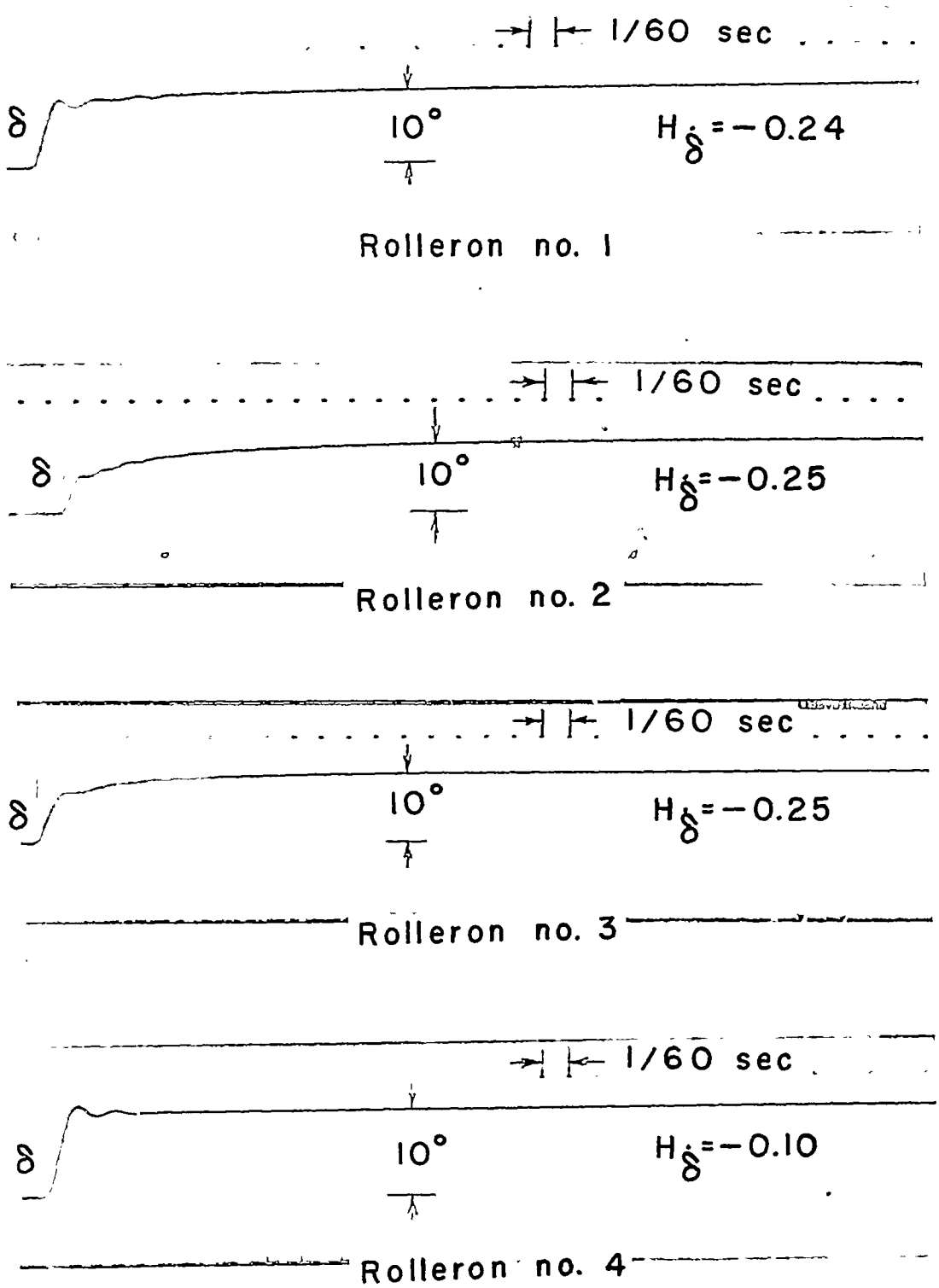

Figure 15.- Rolleron control-surface transient responses indicating damping characteristics of orifice damper for model B.

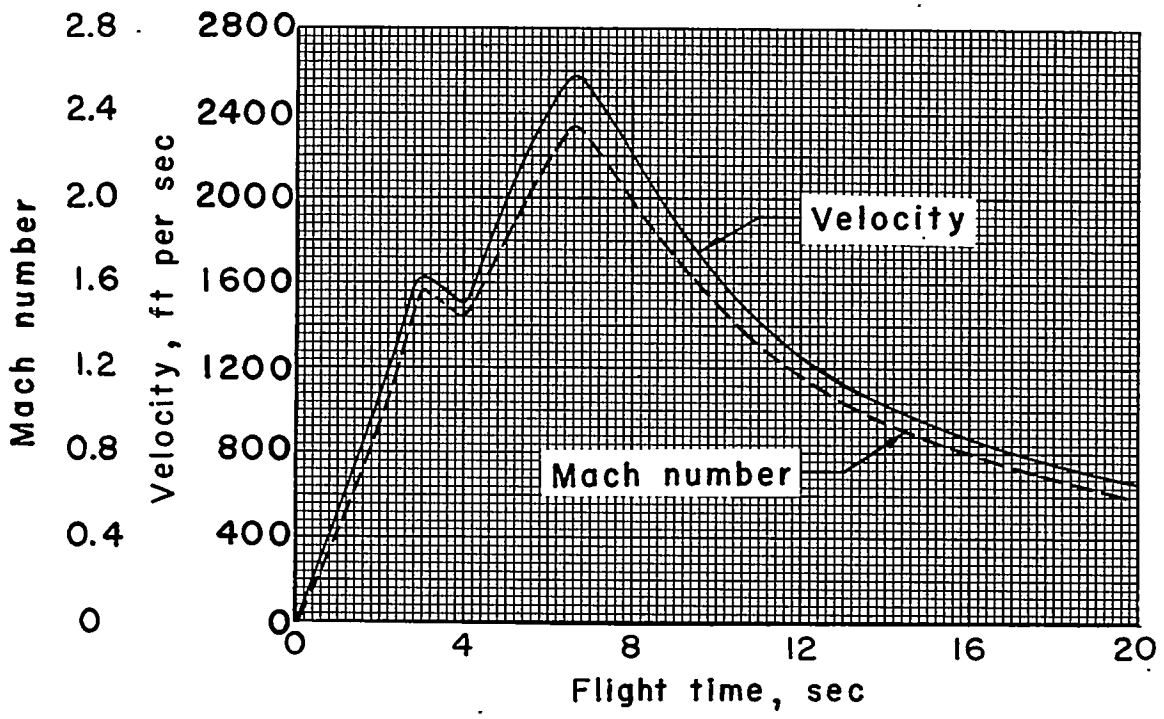

(a) Model A.

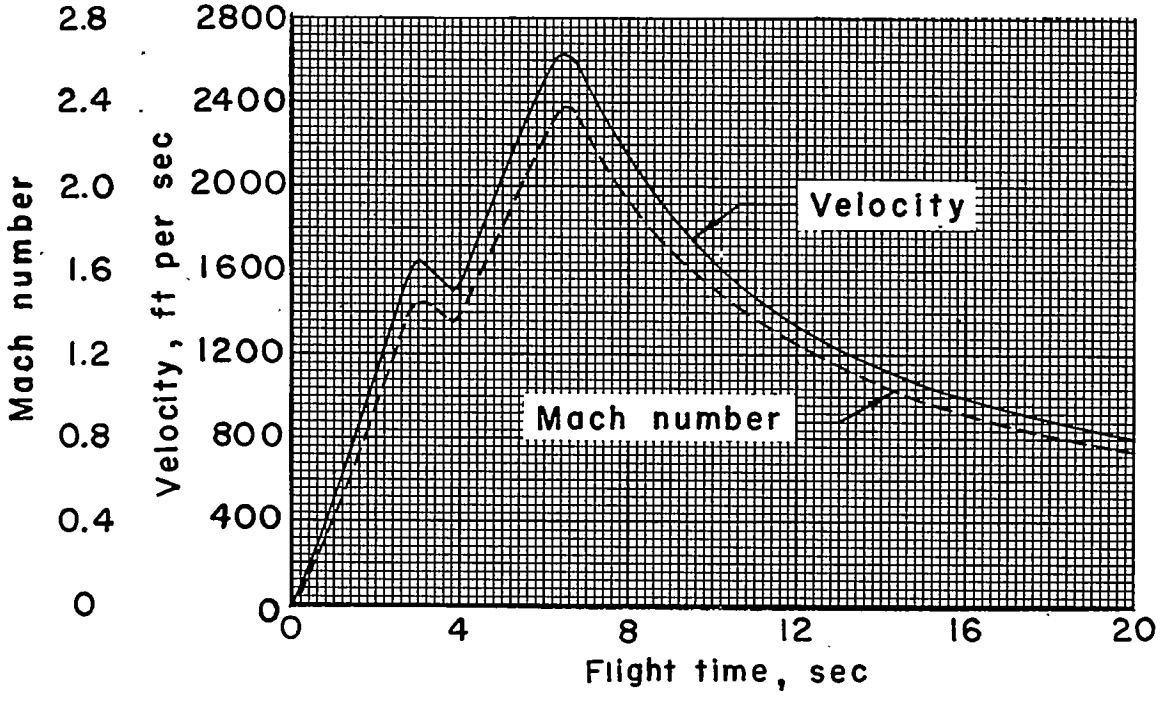

(b) Model B.

Figure 16.- Variation of velocity and Mach number with flight time for models A and B.

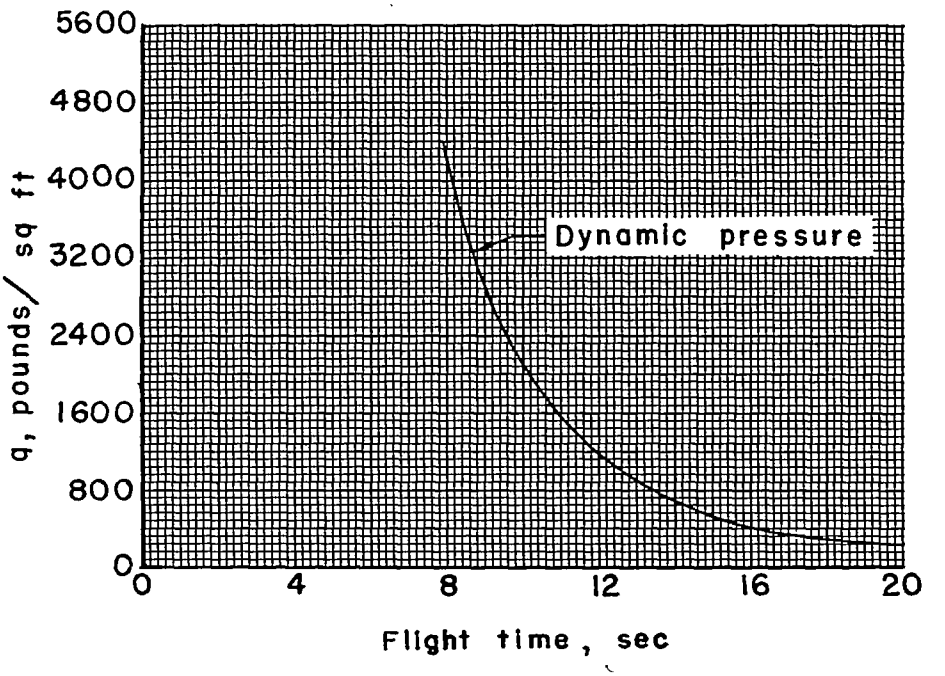

(a) Model A.

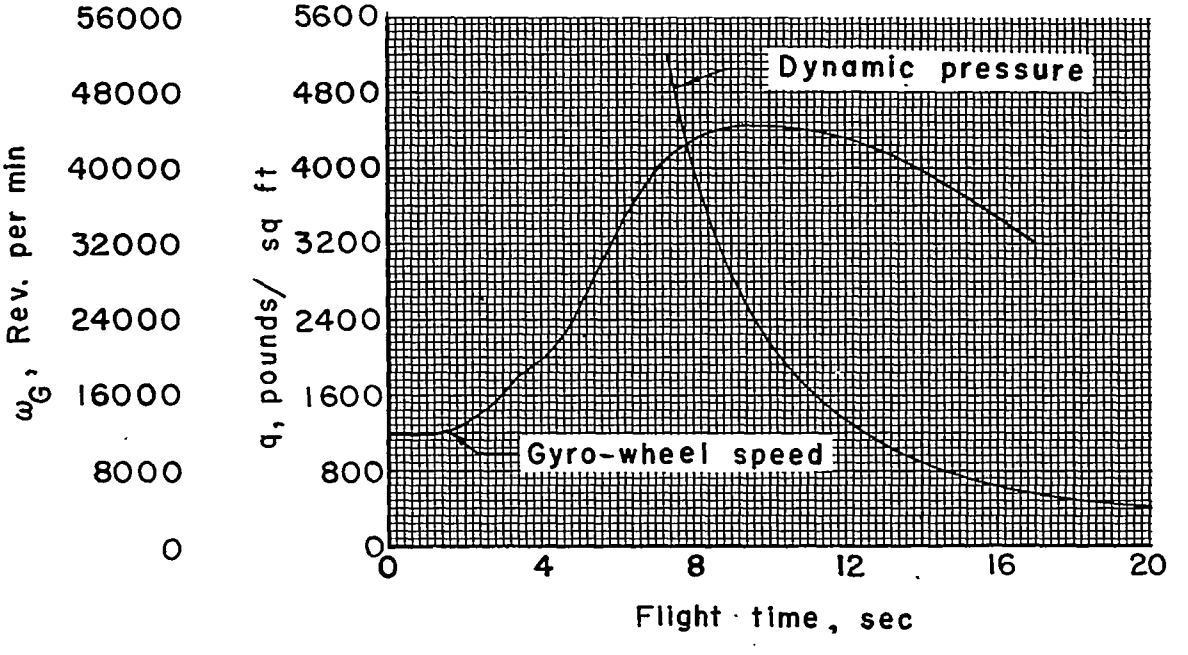

(b) Model B.

Figure 17.- Variation of dynamic pressure and gyro-wheel speed with flight time for models A and B. Gyro-wheel speed was measured only on model B.

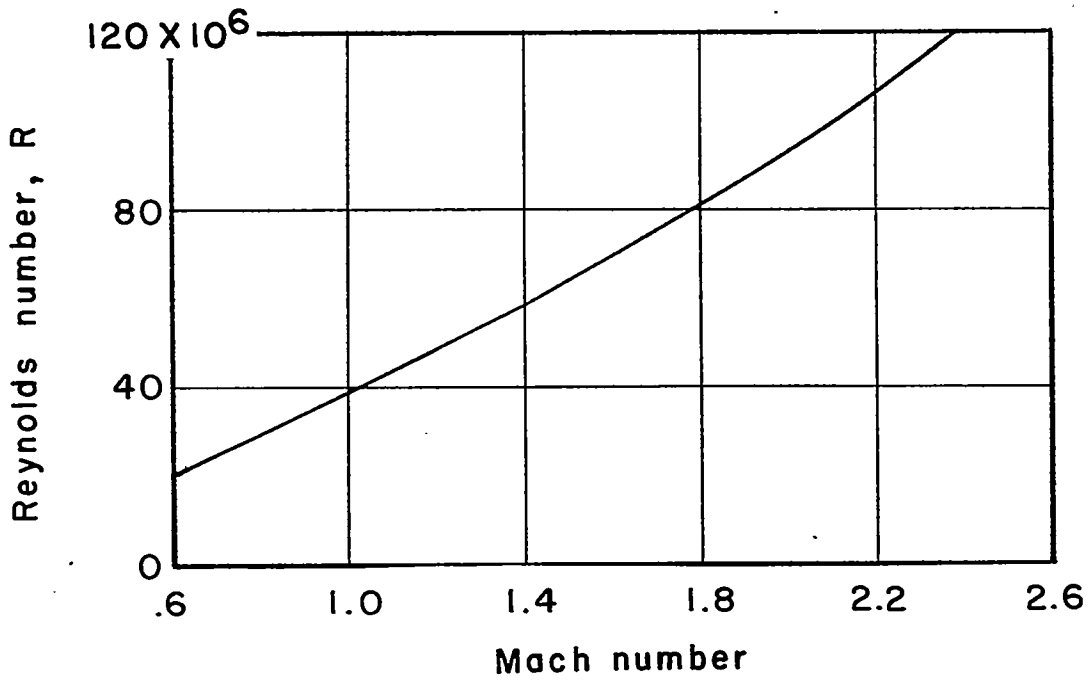

(a) Model A.

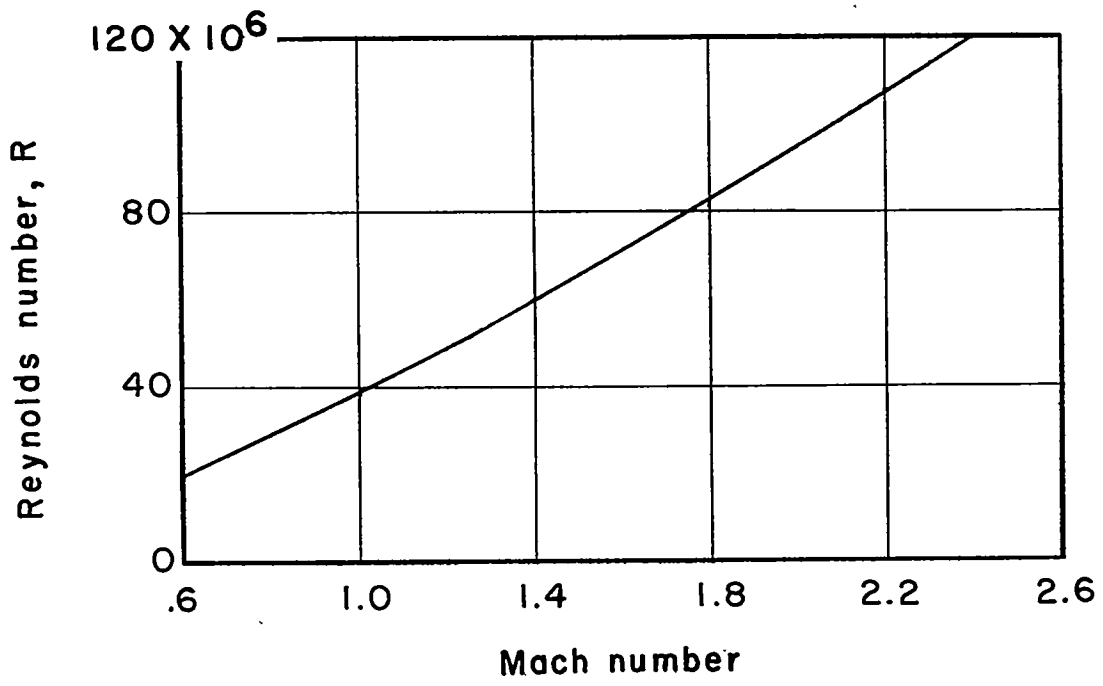

(b) Model B.

Figure 18.- Variation of Reynolds number, based on missile length, with Mach number for models A and B.

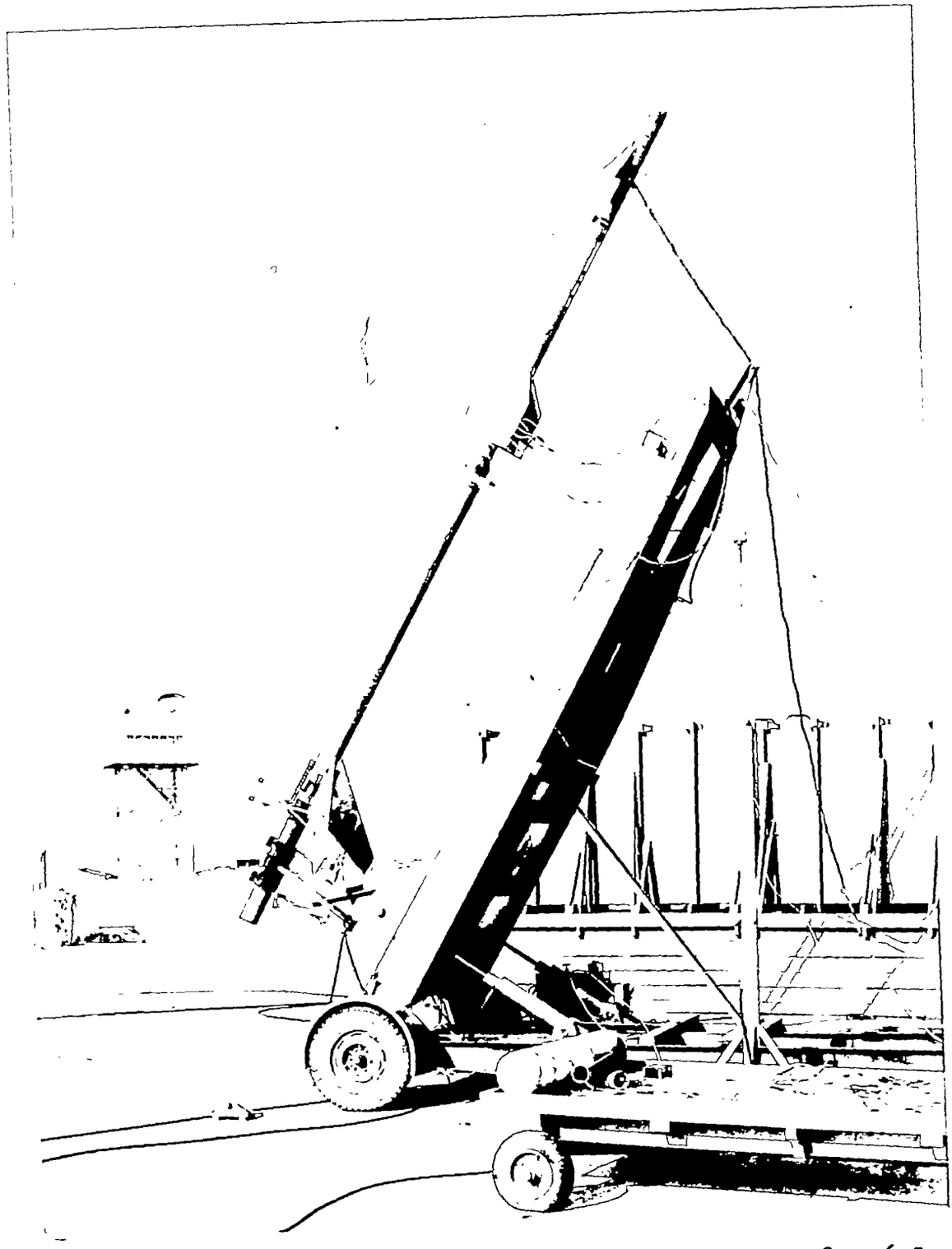

L-82276.1

Figure 19.- Photograph of model and booster prior to launching.

CONFIDENTIAL

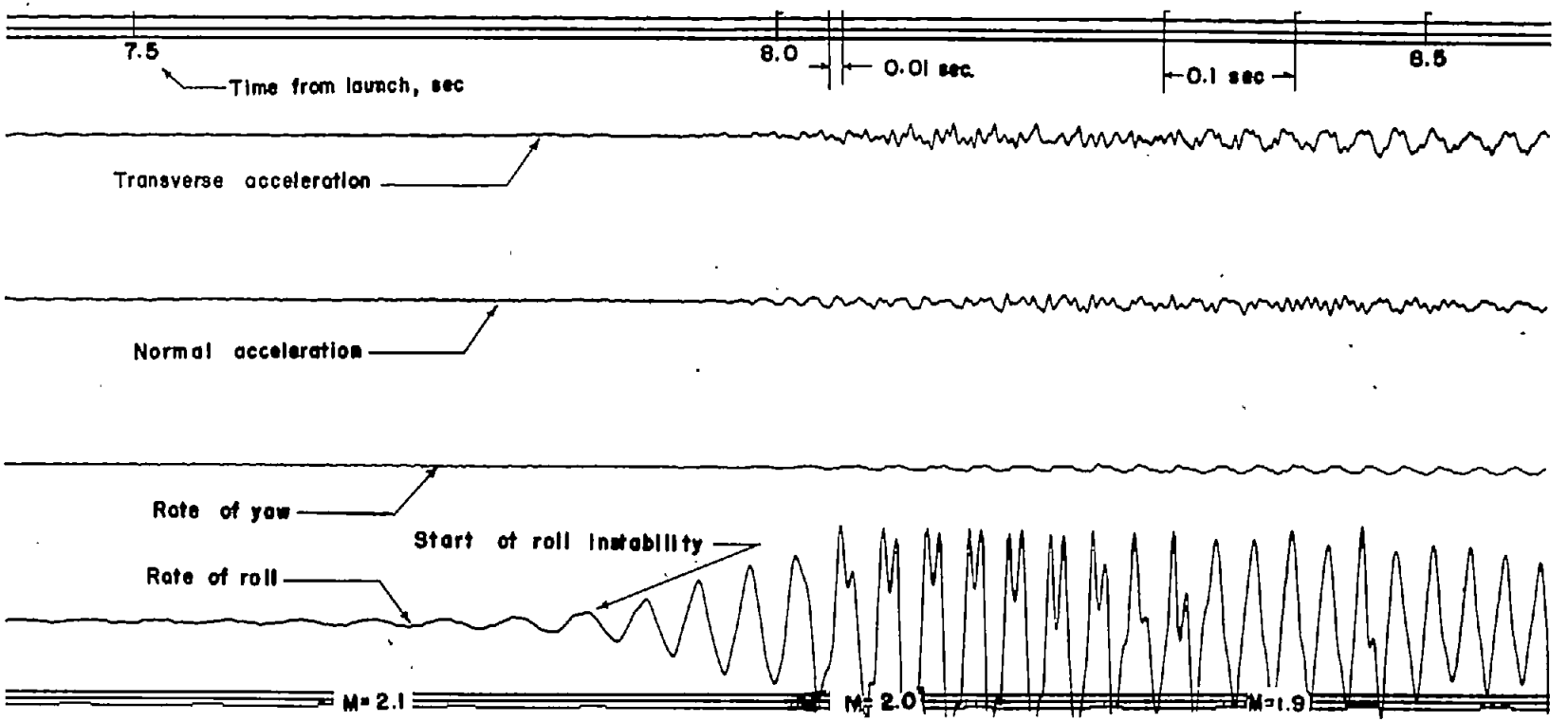

(a) Time, 7.5 to 8.5 seconds.

Figure 20.- Reproduction of portions of uncalibrated telemeter record obtained from the flight test of model A.

CONFIDENTIAL

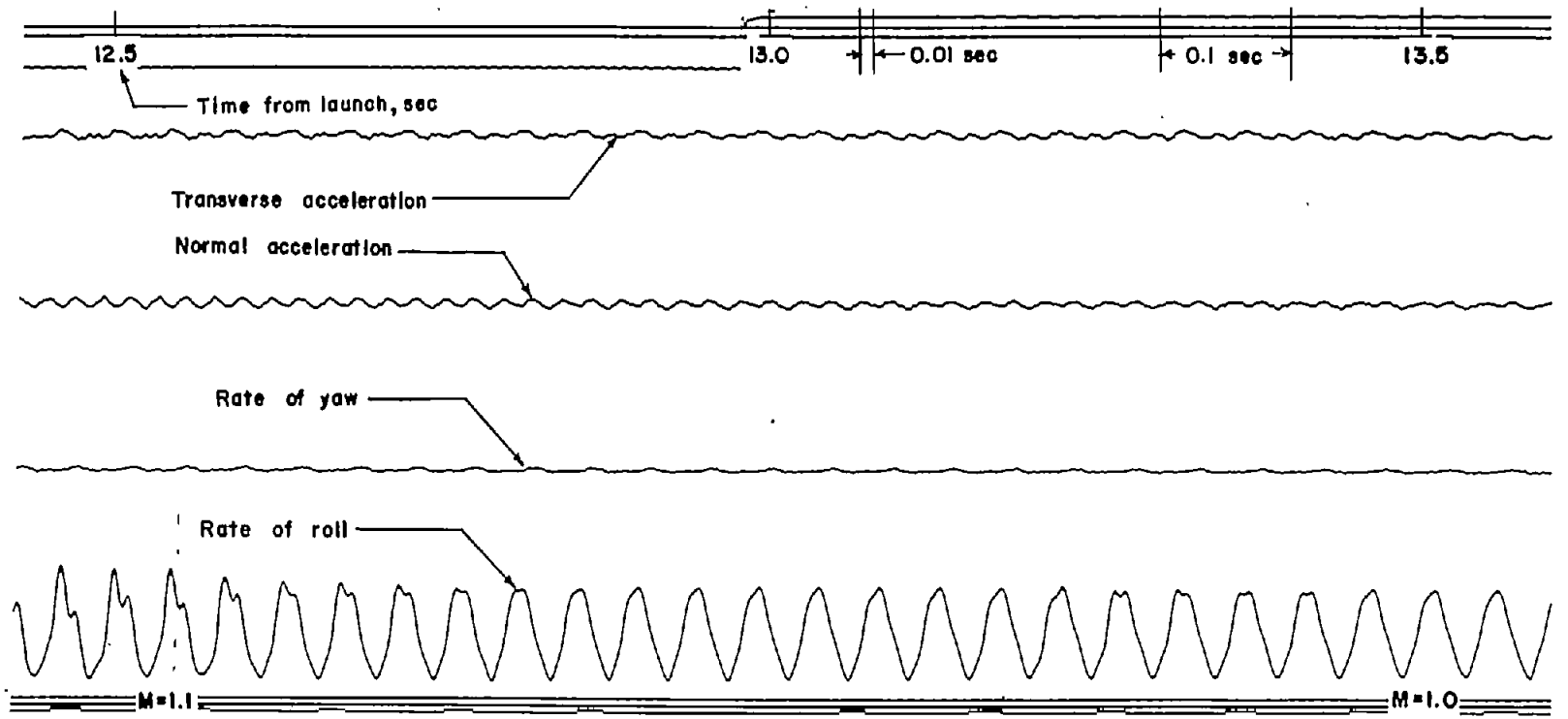

(b) Time, 12.5 to 13.5 seconds.

Figure 20.- Continued.

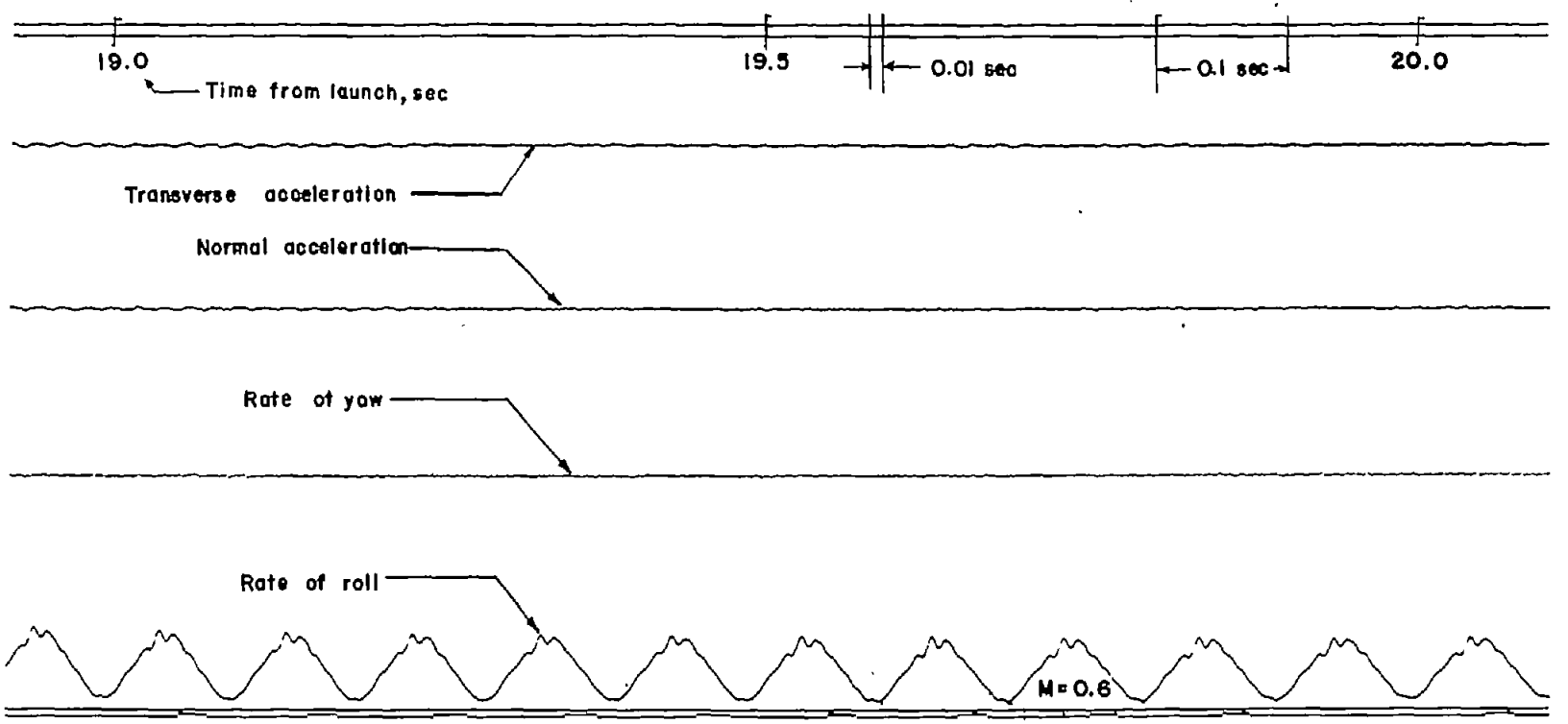

(c) Time, 19.0 to 20.0 seconds.

Figure 20.- Concluded.

CONFIDENTIAL

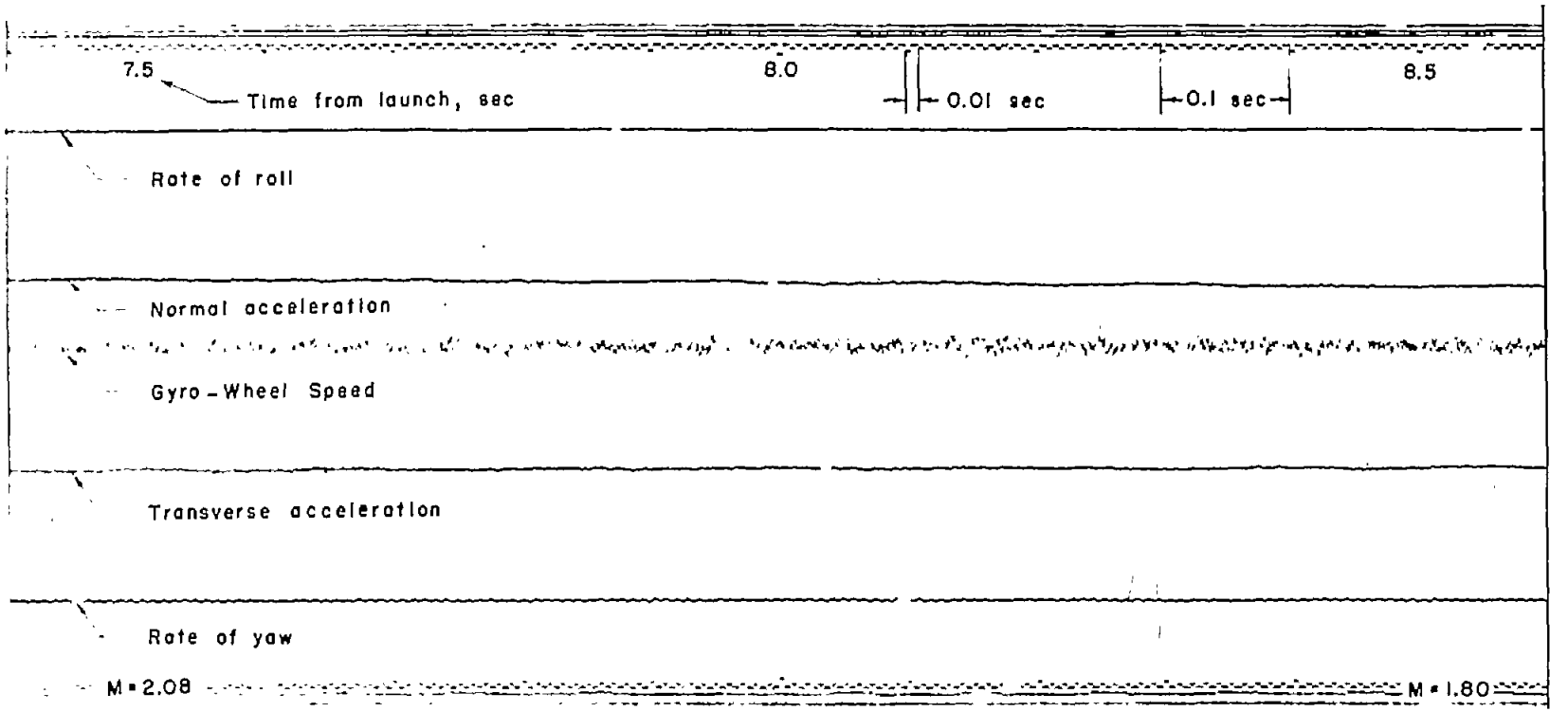

(a) Time, 7.5 to 8.5 seconds.

Figure 21.- Reproductions of portions of uncalibrated telemeter record obtained from the flight test of model B.

CONFIDENTIAL

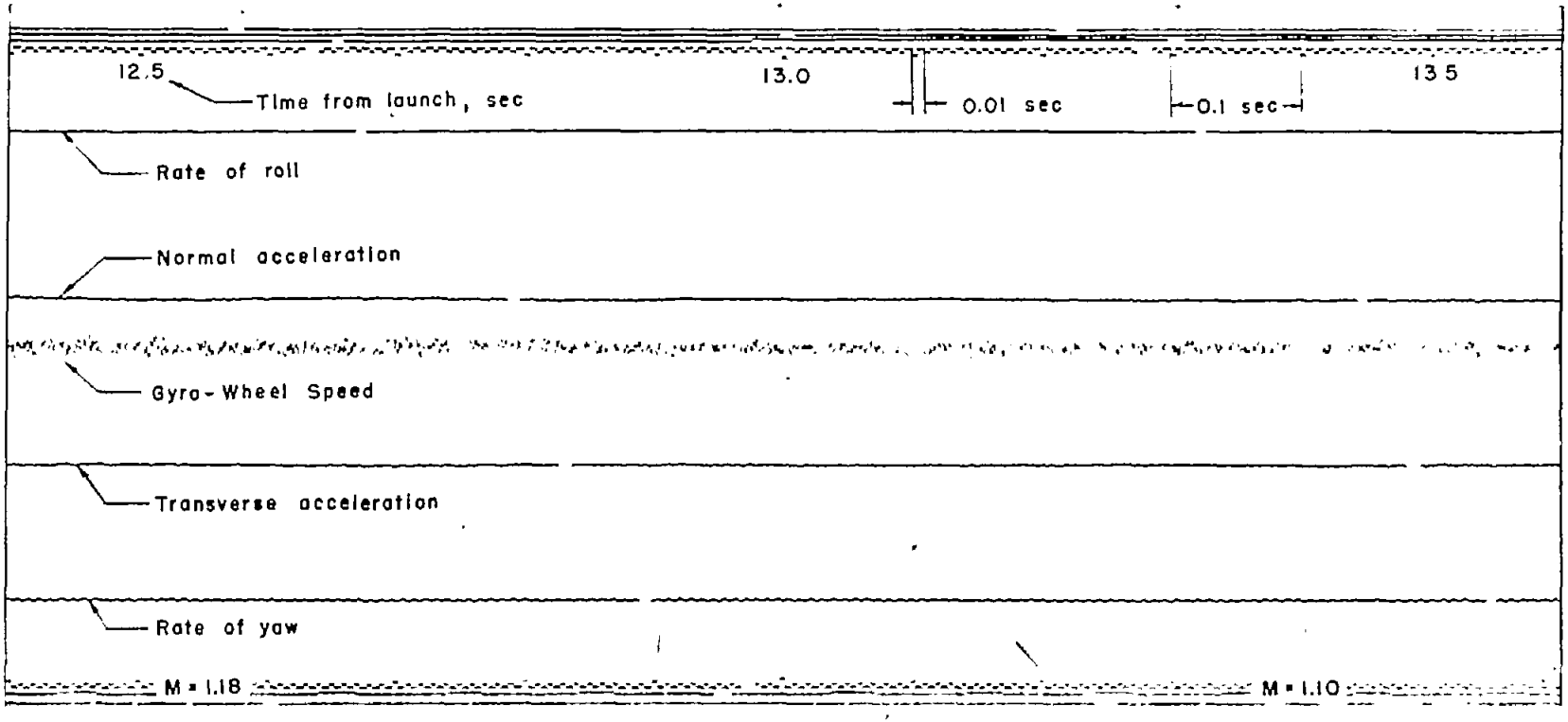

(b) Time, 12.5 to 13.5 seconds.

Figure 21.- Continued.

CONFIDENTIAL

CONFIDENTIAL

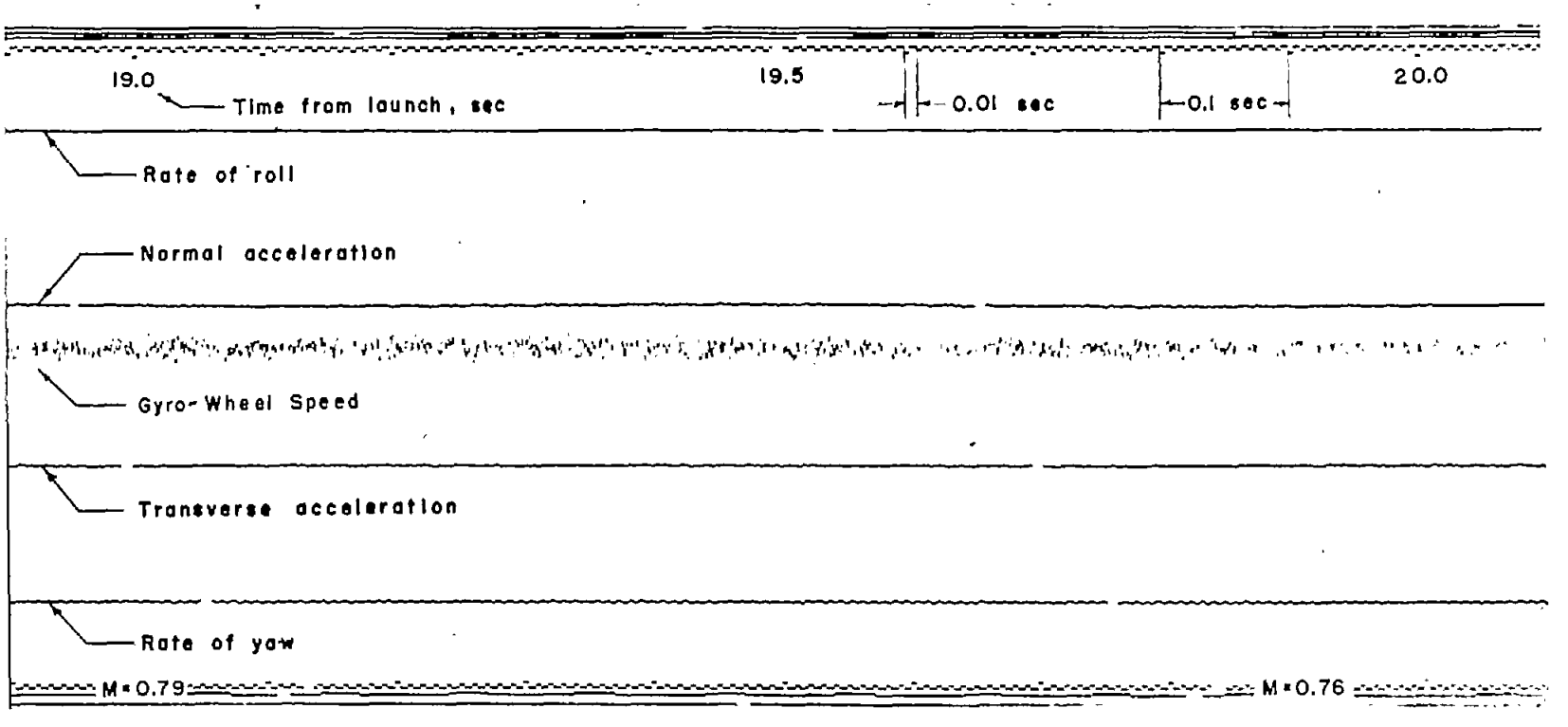

(c) Time, 19.0 to 20.0 seconds.

Figure 21.- Concluded.

CONFIDENTIAL

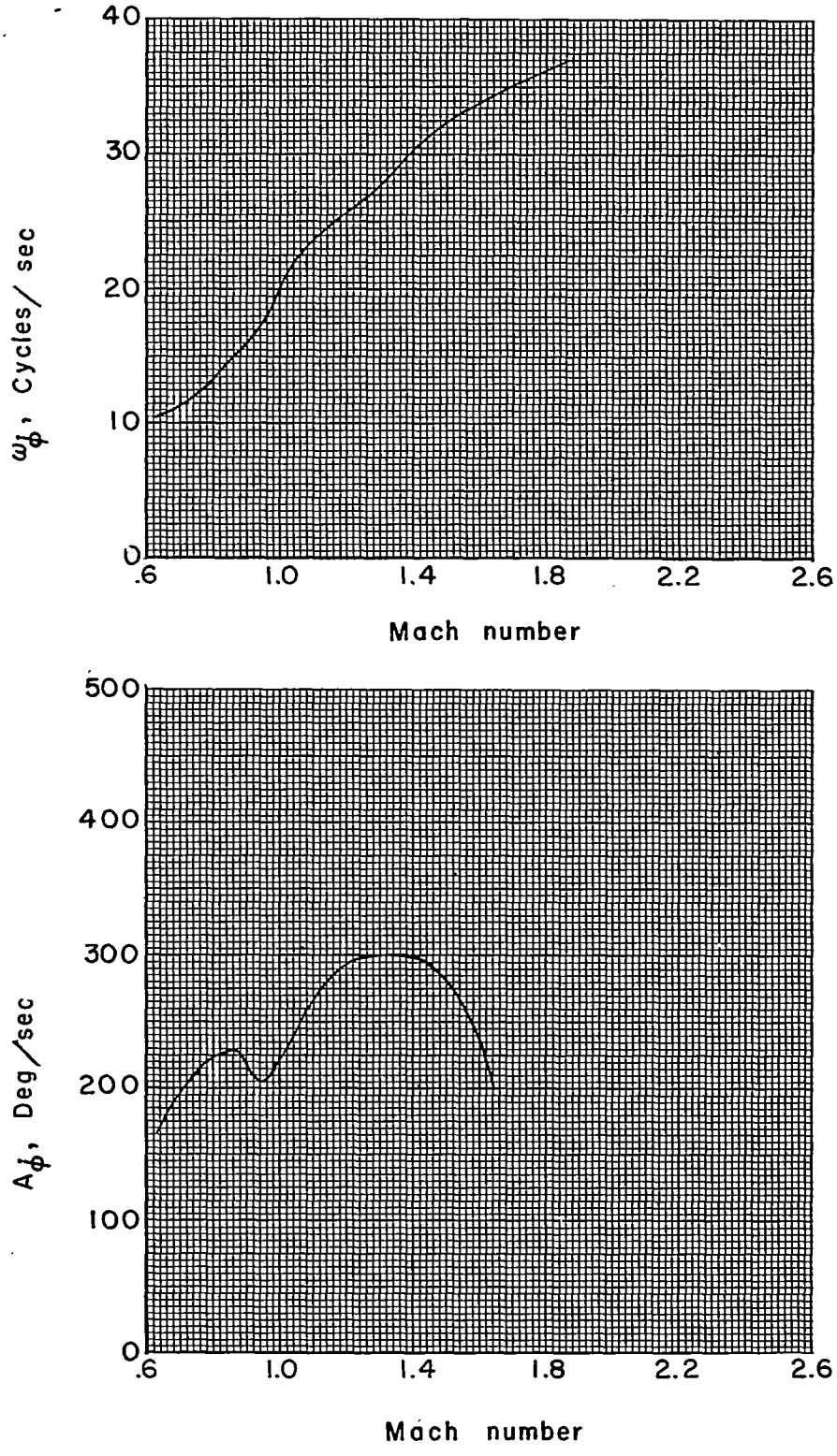

Figure 22.- Variation of half-amplitude and frequency of self-sustained roll oscillation with Mach number for model A.

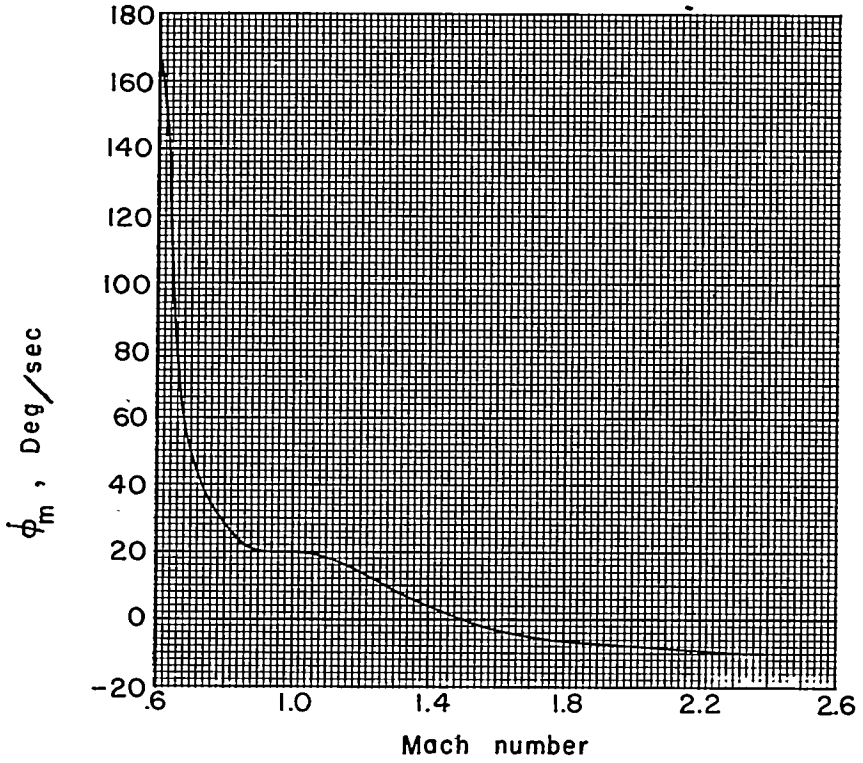

(a) Model A.

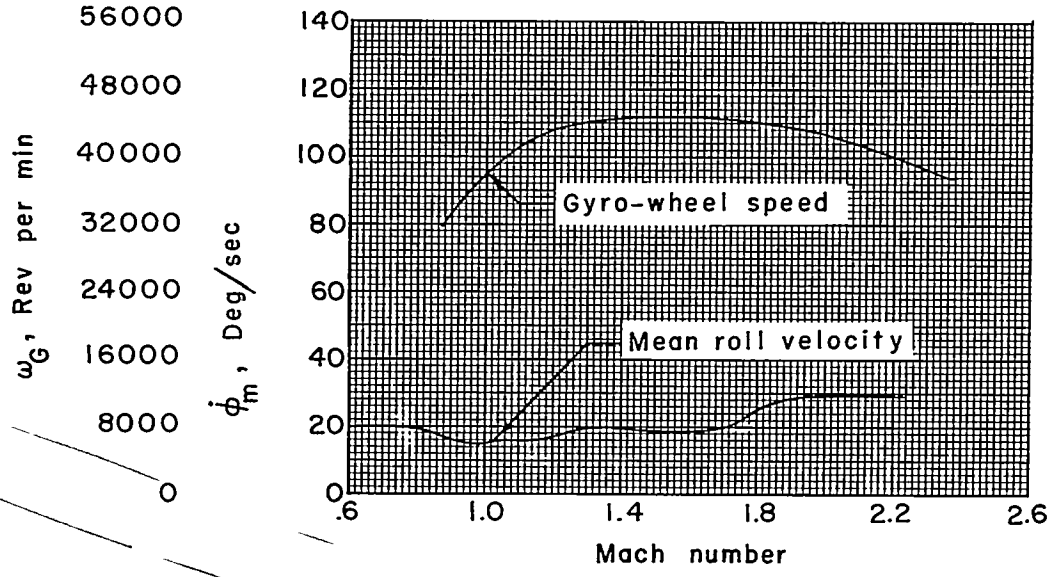

(b) Model B.

Figure 23.- Mean roll velocity and gyro-wheel angular-speed variation with Mach number for models A and B. The gyro-wheel speed was measured only on model B.

CONFIDENTIAL

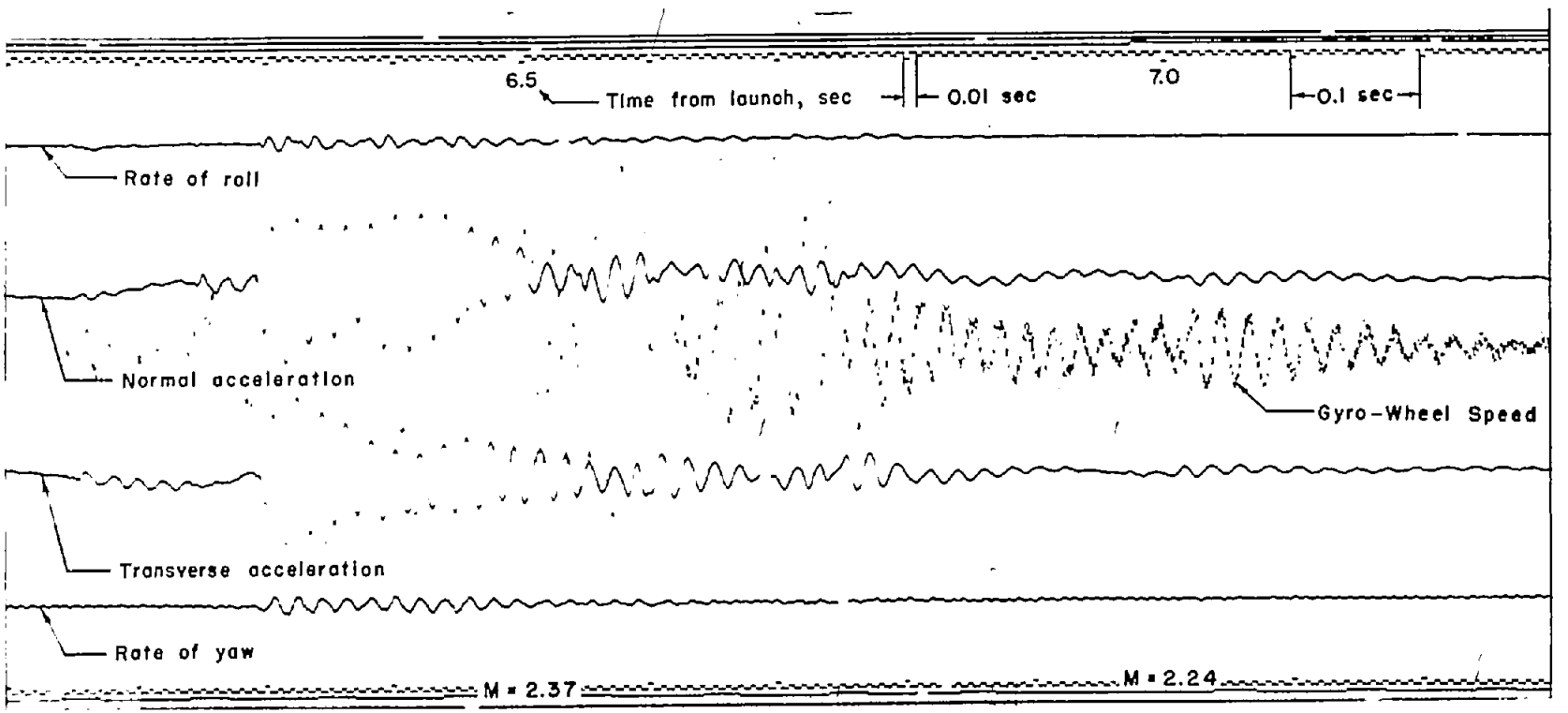

Figure 24.- Reproduction of uncalibrated telemeter record near sustainer-rocket-motor burnout for model B showing longitudinal oscillation.

CONFIDENTIAL

NACA - Langley Field, Va.